



Technische Universität München
School of Computation, Information and Technology
Bio-Inspired Information Processing

Bachelor's Thesis

Investigation of Cortical Responses to Modulated Noise Stimuli Using fNIRS

Pei-Yi Lin

Date of Submission:
September 18, 2022

Supervisors:
Prof. Dr.-Ing. Werner Hemmert
Dr. Ali Saeedi
M.Sc. Carmen Marie Castañeda González

Abstract

In this study, we sought to determine whether functional near-infrared spectroscopy (fNIRS), a non-invasive neuroimaging method that is safe to use repeatedly and for an extended period of time, can provide an objective measure of the cortical response when subjects are exposed to different levels of sound intensity. Eight normal-hearing subjects, including both biological genders and different races, were included and actively participated in the present study. Measurement data were processed to compute the changes in oxyhemoglobin and deoxyhemoglobin concentration. The resulting waveform morphologies were studied and a regional analysis was conducted. The results were compared with previous studies, mainly the one from Weder et al. (2018). Potential reasons to cause the variance from the previous research (Weder et al., 2018) were investigated. The feasibility of using fNIRS for neuroimaging in hearing research was once again evaluated.

Keywords— functional near-infrared spectroscopy, cortical responses, sound intensities , language processing , normal-hearing listeners

Acknowledgments

Huge thanks to my friends who volunteered and participated in this study.

Contents

1	Introduction	1
1.1	Motivation	1
1.2	Technical Background	2
1.3	Related Work	4
2	Methods	6
2.1	Study Participants	6
2.2	Probe Design	6
2.3	Acoustic Stimulation during fNIRS Experiment	10
2.4	fNIRS Setup	13
2.5	Data Procesing	14
3	Results	18
3.1	Participant 3	20
3.2	Participant 4	22
3.3	Participant 5	24
3.4	Participant 7	26
4	Discussion	28
4.1	Waveform Morphology	28
4.2	Regional Analysis	28
4.3	Device Limitation and fNIRS Testing Conditions	29
4.4	Data Processing	30
4.5	Loudness Perception	31
4.6	Intelligibility of the Auditory Stimuli	31
4.7	Language Processing in Human Brains	31
4.8	Laterality of Brain Activation	32
4.9	Depth and Location of Cortical Response	32
4.10	HbR and HbO Data	33
5	Conclusion and Future Prospectives	34

Contents

A Acronym	36
B List of Figures	39
C List of Tables	42
D Other Measurement Data	44
D.1 Participant 1	44
D.2 Participant 2	46
D.3 Participant 6	48
D.4 Participant 8	50
References	55

Chapter 1

Introduction

1.1 Motivation

This research aims to better understand the brain activities of normal-hearing subjects when they are exposed to auditory stimuli of different loudness with the help of functional near-infrared spectroscopy (fNIRS).

In the field of neuro-imaging, although functional magnetic resonance imaging (fMRI) is widely used and provides excellent resolution, it still has many limitations, especially when it comes to hearing research. First of all, the fact that fMRI rooms are noisy makes it difficult to control the desired auditory stimulation due to inevitable environmental noises. In addition, fMRI scans are done in a magnetic field. It has not yet been proved that pregnant women and infants can be safely exposed to an external magnetic field in the fMRI room. For people with hearing disabilities, more specifically cochlear implant patients, going into a fMRI room would not be ideal, either. Although there are already cochlear implants that can be worn to a magnetic field, it is still generally not suggested to wear a piece of metal in a fMRI room.

With fNIRS, we can measure brain activity by using near-infrared light to estimate cortical hemodynamic activities which occur in response to neural activity. It is non-invasive and risk-free. The fNIRS device is portable and works silently. With the cap secured on the head, it is also more resilient to motion artifacts. All of these makes it ideal for hearing research. However, it is not yet commonly used in clinical diagnostics due to the lack of understanding of the expected brain activities measured with fNIRS. In addition, the spatial resolution is also worse than that of fMRI. Therefore, in this research, we performed some fNIRS measurements, processed and analysed the fNIRS recording data under different experiment conditions, in

Introduction

hope of relating and better interpreting the relationship between the actual brain activities and the fNIRS recordings.

If we can utilize fNIRS better so that the technology can be more commonly used in clinical applications, hearing abnormalities of patients can be diagnosed earlier. This is especially important for infants or children. There is strong evidence that language development happens in the early stages of one's life (Newport, 1990), and children may never acquire a language if they have not been exposed to a language before they reach the age of six or seven (Clark, 2000). As a result, early identification and intervention of hearing loss can prevent severe linguistic, communicative, and psychosocial repercussions (Robinshaw, 1995) (Yoshinaga-Itano et al., 1998). Hearing research a meaningful topic. For one, speech is the primary and direct way of human communication. We express ourselves and perceive other people's opinion via speech. For the other, music is an important part of humanity. It provides a means of symbolic representation of emotions and ideas. Without the ability to hear and listen, neither speech nor music will be possible to be perceived. Therefore, helping other people with hearing disabilities get better diagnosis and treatment is the ultimate goal for this study, and fNIRS is of great potential to help solve the issue.

1.2 Technical Background

The central concept of fNIRS neuroimaging is dependent on the relationship between oxygen consumption and the neuronal activity. Increases in neuronal activity require more glucose and oxygen to be rapidly delivered via the bloodstream. Hemoglobin, the protein from inside red blood cells, transports oxygen molecules throughout the body. Higher hemoglobin levels and red blood cell transfusion are associated with higher cerebral oxygen delivery. Via this hemodynamic response, the blood releases glucose and oxygen to active neurons at a faster rate relative to inactive neurons (Pelphrey, 2013). Different concentration levels of hemoglobin results in a spectral change of light absorption. The biological tissue has relatively good transparency for light in the near-infrared region (700-1300nm) (Jöbsis, 1977), so it is possible to transmit sufficient photons. By measuring this blood-oxygen-level-dependent (BOLD) signal, fNIRS neuroimaging is, therefore, possible *in situ* monitoring.

1.2 Technical Background

The technique of fNIRS relies on the Beer-Lambert law (Swinehart, 1962), which is given by:

$$OD_\lambda = \log\left(\frac{I_0}{I}\right) = \epsilon_\lambda \cdot c \cdot L \quad (1.2.1)$$

OD_λ : a dimensionless factor known as the optical density of the medium.

I_0 : the incident radiation.

I : the transmitted radiation.

ϵ_λ : the molar absorptivity ($mM^{-1} \cdot cm^{-1}$) of the chromophore.

c : the concentration (mM) of the chromophore.

L : length of the light path.

The Beer-Lambert law applies to a clear, non-scattering medium. When the law is applied to a scattering medium, e.g. brain tissue, a correction factor should be applied. The factor, called differential path length factor (DPF), accounts for the increase in optical path length due to scattering in the tissue. The modified Beer-Lambert law (Delpy et al., 1988) is given by:

$$OD_\lambda = \epsilon_\lambda \cdot c \cdot L \cdot B + OD_{R,L} \quad (1.2.2)$$

where $OD_{R,L}$ represents the oxygen-independent light absorption due to scattering in the tissue, and $(L \cdot B)$ is the true mean path length traveled by the detected photons. In our case, i.e. CW-NIRS ¹, the mean path length is not known. In a highly scattering medium, the path length of trajectories is longer than the source-detector separation. Nevertheless, one can still estimate the path length within the whole sampling region by multiplying the source-detector distance with a DPF. Assuming $OD_{R,L}$ is constant during a measurement, we can rewrite the previous equation in terms of changes in optical density and changes in concentration as follows:

$$\Delta c = \frac{\Delta OD_\lambda}{\epsilon_\lambda \cdot L \cdot B} \quad (1.2.3)$$

The validity of the above equation depends on how much the DPF, or in this equation "B" varies. (Delpy et al., 1988) investigated this question and gave a relation between the DPF and the head diameter. Newer research also provides different ways to estimate the DPF. In the scope of this present study, the DPF was calculated from a function of wavelengths of the emitted photons from the source and the age of the participant (Duncan et al., 1996).

¹The Continuous Wave (CW) method relies on the steady illumination of tissue and the detection of the transmitted light intensity. This conceptually and technically simplest form of tissue spectroscopy assesses the overall light attenuation inside the tissue and cannot differentiate effects of scattering and absorption. Source : <https://nirx.net/cwfnirs>

Introduction

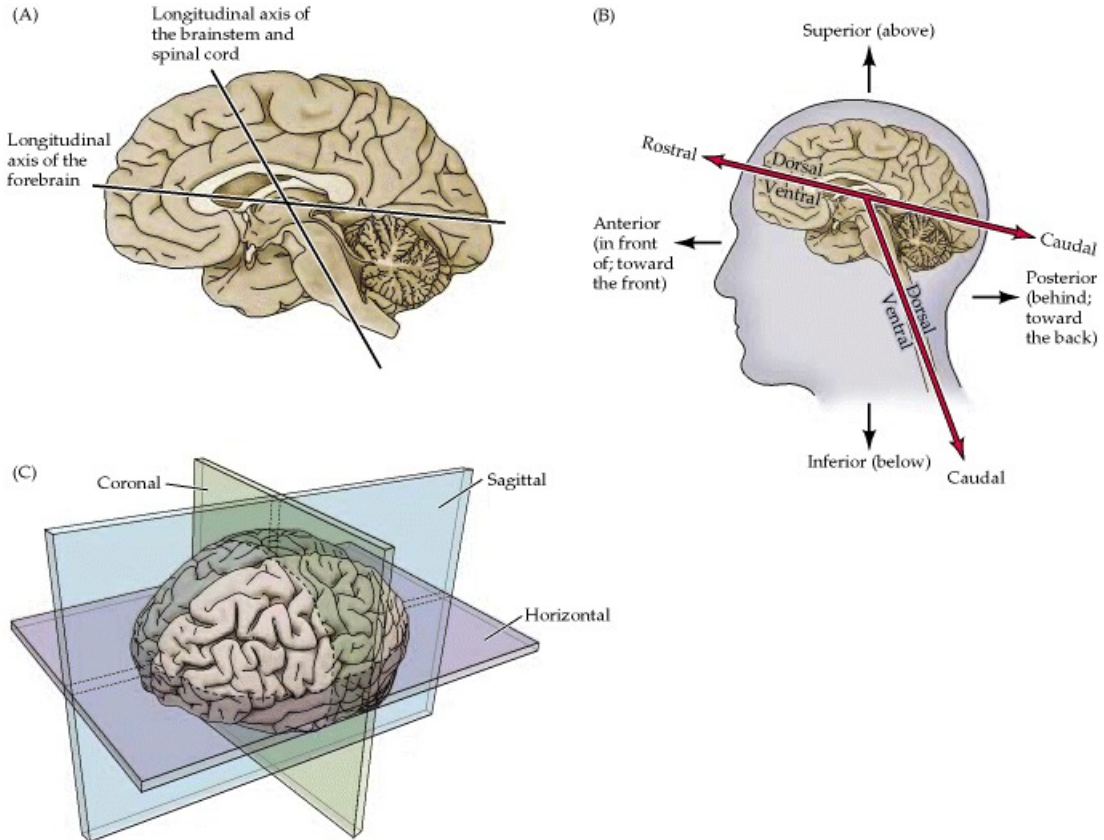
1.3 Related Work

Despite the fact that fNIRS has become a popular neuroimaging method for hearing research, spatial resolution is reduced compared to fMRI, and often the exact locations of fNIRS optodes and detailed anatomical information is not known. On top of the limited spatial resolution of fNIRS, the relationship between cortical activation and speech processing is not yet clearly investigated, either. Until now, there are no standard fNIRS source-detector locations that are generally accepted as being ideal for capturing cortical activation in response to speech signals. As a result, many research was done to overcome the aforementioned limitations and enable fNIRS in more clinical practice.

Frost et al. (1999) conducted a fMRI study and found evidence that language processing is strongly left lateralized in both sexes. Belin et al. (2000) also used fMRI and found that the superior temporal sulcus (STS) showed greater neuronal activity when subjects listened passively to vocal sounds, whether speech or non-speech, than to non-vocal environmental sounds. Shader et al. (2021) explored broad and restricted regions of interest that are sensitive to detecting cortical activation using fNIRS in response to auditory- and visual-only speech stimuli with fNIRS. Their results suggested that temporal regions near Heschl's gyrus may be the most advantageous location in adults for identifying hemodynamic responses to complex auditory speech signals using fNIRS. Pollonini et al. (2013) studied the cortical activation level in response to the speech signals with different levels of intelligibility. Their fNIRS evidence measurements showed that normal speech evoked stronger responses within the auditory cortex compared to distorted speech. Environmental sounds produced the least cortical activation.

This project is based on a previous study (Weder et al., 2018). The authors measured human subjects with fNIRS when the subjects were given different sound stimuli with different sound pressure levels. In their research, the results showed that fNIRS responses originating from auditory processing areas are highly dependent on the sound intensity level. More specifically, higher stimulation levels led to larger concentration changes of oxyhemoglobin and deoxyhemoglobin. Caudal and rostral channels showed different waveform morphologies, reflecting specific cortical signal processing of the stimulus.

1.3 Related Work



Source: <https://www.ncbi.nlm.nih.gov/books/NBK10971/>
visited in September 2022.

Figure 1.1: Anatomical terminology.

See (B). The terms anterior, posterior, superior, and inferior refer to the long axis of the body, while the terms dorsal, ventral, rostral, and caudal refer to the long axis of the central nervous system. Source: <https://www.ncbi.nlm.nih.gov/books/NBK10971/>
visited in September 2022.

Chapter 2

Methods

2.1 Study Participants

We measured eight normal-hearing people. Participant 8 was given silent stimuli as a comparison. Detailed information about the subjects is listed in Table 2.1.

Participant	Gender	Handedness	Race	Hair color	Age (year)
1	F	right-handed	east asian	dark	22
2	M	right-handed	caucasian	blond	18
3	M	left-handed	caucasian	brunet	21
4	F	right-handed	east asian	dark	21
5	M	right-handed	caucasian	blond	26
6	F	right-handed	southeast asian	dark	22
7	M	left-handed	east asian	dark	23
8	M	right-handed	caucasian	blond	22

Table 2.1: Demographic information of the study participants.

2.2 Probe Design

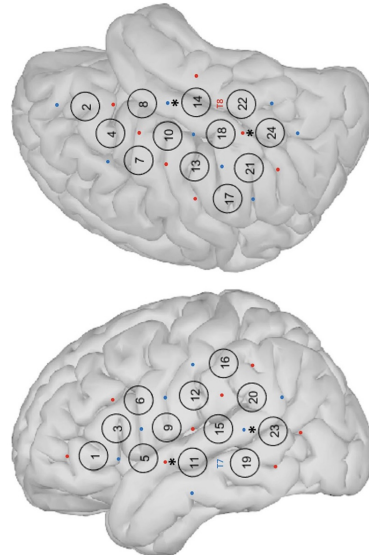
The probes were first designed in AtlasViewer (release v2.11.3 ¹) (see Figure 2.2) (Aasted et al., 2015) and the SD GUI interface ² (see Figure 2.4). The probe design was made as close as possible to the research from Weder et

¹<https://github.com/BUNPC/AtlasViewer/releases/tag/v2.11.3>

²a sub GUI of AtlasViewer

2.2 Probe Design

al (2018). However, several modifications had to be made due to the device limitations.



Source: <https://link.springer.com/article/10.1007/s10162-018-0661-0>

Figure 2.1: Probe design from Weder et al. (2018)

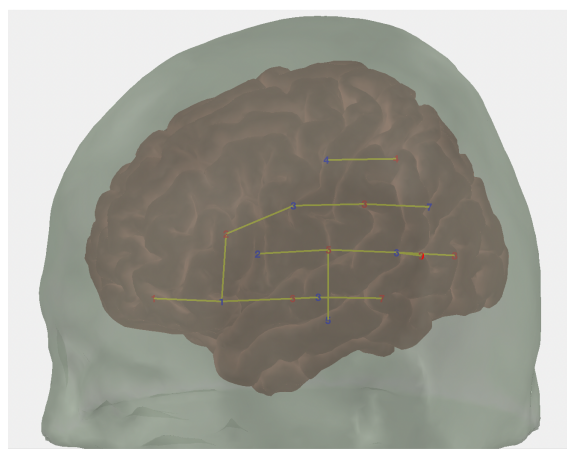
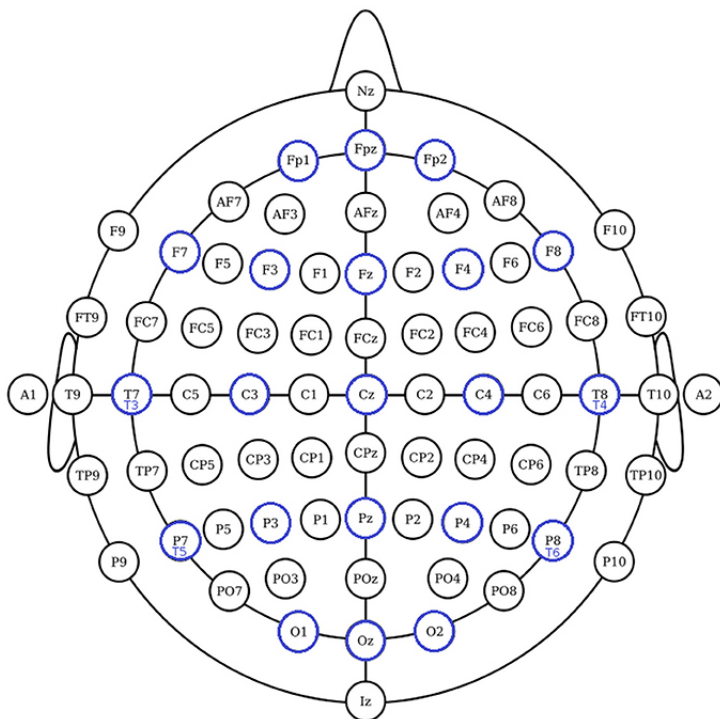


Figure 2.2: Probe design in this research. The original view is shown here in AtlasViewer. The red numbers represent the light sources and the blue numbers represent the detector. Channels are shown in yellow lines. For better readability, our channel definition will be shown later in the report in another edited picture (Figure 3.1) from AtlasViewer.

Methods

First of all, the paper only provided a rough 2D sketch of their probe design (see Figure 2.1). The exact channel positions were not described in detail. Although there are different ways to define the channels, we believe it does not matter as long as the mid-points of the channel corresponding to that of the previous research (Weder et al., 2018).



Source: <https://www.frontiersin.org/articles/10.3389/fnins.2018.00235/full>

Figure 2.3: The 10-10 international system of EEG electrode placement. T7 is the left 10% position between A1 and A2 through the central Cz.

Side note: 10-20 System is shown in blue. T7 in the 10-10 system is exactly T3 in the 10-20 system.

2.2 Probe Design

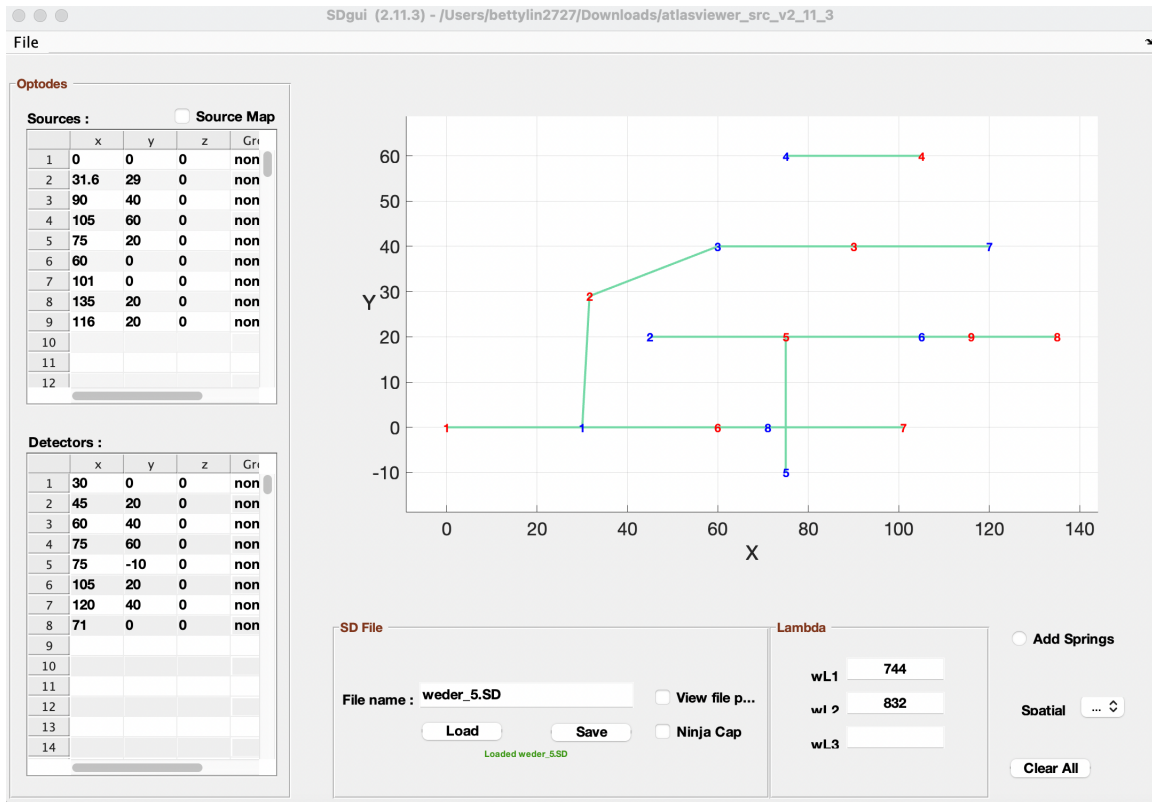


Figure 2.4: SDgui interface and optode coordinates.

Due to device limitations, we only measured one side of the brain. According to Frost et al. (1999) , language processing has been predominantly associated to cortical activity in the left hemisphere. As a result, we decided to put more focus on the left hemisphere.

The fNIRS device we used also had limited number of sources and detectors. In the original design of Weder et al. (2018), 9 sources and 9 detectors were used. However, the device we used had only 10 sources and 8 detectors. Hence, we shifted one channel around T7 (see Figure 2.3) a little bit to the left. More specifically, instead of putting another detector on the position T7, we defined a channel between source 7 and detector 8 (see Figure 2.4), so that one less detector is needed. At the end, there were 12 long channels and 2 short channels (channel 11 and 13 are short channels) in our setup (see Figure 3.1).

Methods

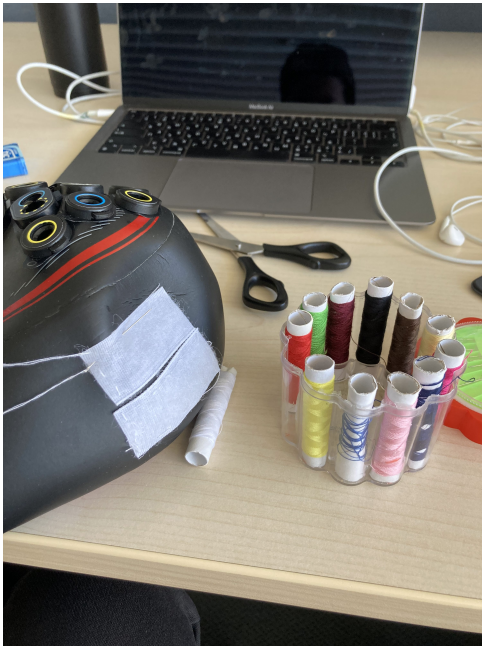


Figure 2.5: Manufacturing process of the cap



Figure 2.6: Finished cap on dummy

The physical cap was self-made from a swimming cap (see Figure 2.6 2.5). With the help of a dummy head model, correct positions of the optodes were marked and holes were drilled accordingly. The mounts were put on the cap on the holes. In order to ensure the length of the long channels to be fixed exactly at 30 mm, plastic holders were also placed on the long channels. The Brite23 package comes with mounts for short channels. Thus, no plastic holders were needed in the case. The short channels were 11 mm long. The self-made cap worked out well. The contacts between the scalp and the optodes were good thanks to the elastic characteristic of the material.

2.3 Acoustic Stimulation during fNIRS Experiment

Auditory stimuli were delivered binaurally via audiometric headphones (Sennheiser HD 650)³. Stimuli consisted of 20-s chunks of ICRA noise⁴ (Dreschler et al.,

³<https://www.sennheiser-hearing.com/de-DE/p/hd-650/>

⁴The ICRA-Noise has been developed for the International Collegium of Rehabilitative Audiology by the HACTES work group (Hearing Aid Clinical Test Environment standardisation). The purpose was to establish collection of noise signals to be used as background

2.3 Acoustic Stimulation during fNIRS Experiment

2001).

To begin with, ICRA noise was developed to be used as background noise in clinical tests of hearing aids and for measuring characteristics of non-linear instruments. The signals are based on live English speech from the EUROM database (Chan et al., 1995) in which a female speaker is explaining the system of arithmetical notation. The speech signals were sampled at a sampling rate of 44.1 kHz. By composing the speech signals with well defined spectral and temporal characteristics, the resulting signals have long-term spectrums but are completely unintelligible.

We chose to use ICRA noise as stimuli based on several reasons. For one, ICRA noise is a broadband amplitude-modulated signal. By selecting a broadband stimulus, broad cortical auditory areas are activated more strongly compared to a simple static stimulus, e.g. a pure tone with a fixed amplitude. The bandwidth of auditory stimuli is positively correlated with the mean percentage signal change and spread of cortical activation (Hall et al., 2001). A previous fMRI study also manifested that more complex auditory stimuli elicit greater response in most parts of the auditory cortex (Belin et al., 2002). For the other, ICRA noise is a well-known and accessible stimulus. It is also considered an international de facto standard for hearing research. In this way, our results can be directly compared to other research.

As for choosing different sound pressure levels, we picked 40 dB, 65 dB, 90 dB, and a silent stimulus, i.e. 0 dB. Calibrations were performed using an oscilloscope, a G.R.A.S. Power Module Type 12AK⁵, and an artificial ear (G.R.A.S. 43AA)⁶. The artificial ear transforms the sound pressure levels (SPLs) into electric signals, i.e. voltages that can be measured by the oscilloscope. According to the instruction manual of the G.R.A.S. artificial ear, the measured level is 11.19 [$\frac{mV}{Pa}$]. The SPL in dB is defined as

$$SPL[dB] = 20 \cdot \log \frac{P}{P_0}, \text{ where } P_0 \text{ is } 20 \mu\text{Pa} \quad (2.3.1)$$

Hence, the relation between SPL and measured voltage is given by:

$$V = 20\mu\text{Pa} \cdot 10^{\frac{SPL}{20}} \cdot 10^{\frac{Gain}{20}} \cdot 11.19 \frac{mV}{Pa} \quad (2.3.2)$$

The headphone with the artificial ear were set up together in the soundproof

noise in clinical tests of hearing aids and possibly for measuring characteristics of non-linear instruments. Source: <https://icra-audiology.org/Repository/icra-noise>

⁵<https://www.grasacoustics.com/products/power-module/traditional-power-supply-lemo/product/225-12ak>

⁶<https://www.grasacoustics.com/products/ear-simulator-kit/traditional-power-supply-lemo/product/238-43aa>

Methods

cabin (IAC 350, IAC Acoustics, Winchester, UK)⁷ to ensure minimal environmental noise. The output voltages were measured with the oscilloscope. This way, the corresponding amplitude inputs for later MATLAB scripts for the desired SPLs can be determined.

MATLAB (version 2019b) and Oxysoft (version 3.3.33) were used during the measurement. In MATLAB, a chunk in the ICRA audio files was selected. It was multiplied with different amplitude levels to create 4 SPLs and ramped with a 10-ms Hanning window. One epoch consisted of all four stimuli (0dB, 40 dB, 65 dB, and 90 dB) that were played once in random order. After each stimulus, there was a 25-s silence to wait for the hemodynamic response. For each participant, 8 epochs were measured. The stimuli were marked with lab streaming layers⁸ to note which SPL it was. This lab streaming layer also acted as an interface between MATLAB and Oxysoft, so that Oxysoft could mark the time for each stimulus in the measurement data correctly in real-time.

⁷<https://www.iac.ie/audiology-booths/the-350-series-maxi-hearing-booth.564.html>

⁸The lab streaming layer (LSL) is a system for the unified collection of measurement time series in research experiments that handles both the networking, time-synchronization, (near-) real-time access as well as optionally the centralized collection, viewing and disk recording of the data. Source : <https://github.com/sccn/labstreaminglayer>

2.4 fNIRS Setup

The Brite23⁹ was used as the fNIRS device in this research. It is lightweight, has 10 sources and 8 detectors, and can support up to 23 channels. The Brite23 fNIRS device was connected via Bluetooth to the PC and the Oxysoft software. For each measurement, the DPF was calculated depending on the age of the participant. The sampling rate for the fNIRS device was fixed at 50 Hz, for enough resolution but not unnecessarily large in terms of data size.

After the settings in the Oxysoft software were done, the participant was asked to put on the self-made cap. On each optode position, the hair was put aside gently with a Q-tip to ensure better contact between the optodes and the scalp. Then, the participant was asked to put on the headphone and go into the soundproof cabin. The participant was also asked to keep the eyes closed and keep the head still to ensure minimum interference from visual stimulation and motion.



Source: https://neurolite.ch/sites/default/files/Brite23%20Brochure_0.pdf
visited in September 2022

Figure 2.7: fNIRS Device: Brite23

⁹https://neurolite.ch/sites/default/files/Brite23%20Brochure_0.pdf
visited in September 2022

Methods

2.5 Data Processing

Data preprocessing and analysis were executed in MATLAB (Mathworks, the USA) and the Homer3 toolbox. The following steps (see Figure 2.8) were executed.

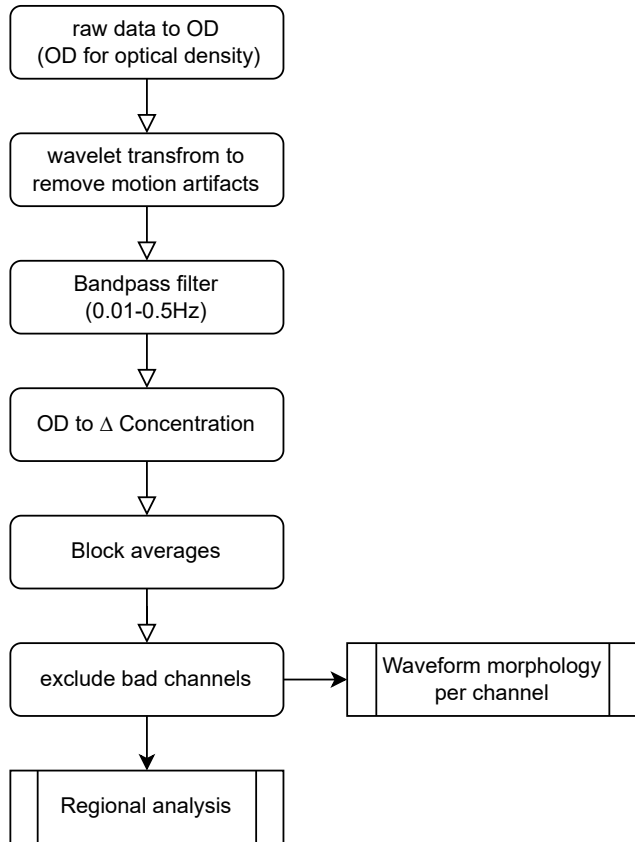


Figure 2.8: Flow chart of data processing steps

First, the hemodynamic response was extracted with the Homer3 toolbox. Raw data were converted into optical densities. Motion artifacts were removed by using wavelet transformation of the data. (Molavi and Dumont, 2012). We also tried to use principle component analysis (PCA) to remove motion artifacts, since PCA has the advantage of faster computation. However, it is also known for tending to remove too much of the activation signal in adults. Wavelet transform, on the other hand, takes longer to compute, but it is better at maintaining relevant frequency content. Then, the Homer3 toolbox bandpass filter (0.01 - 0.5 Hz) was used to reduce drift, broadband noise, heartbeat, and respiration artifacts. Changes in concentration of oxy-

2.5 Data Processing

generated hemoglobin (HbO) and deoxygenated hemoglobin (HbR) were estimated by applying the modified Beer-Lambert Law (Delpy et al., 1988). In this step, a correction factor, DPF, is used. Although strictly speaking, the DPF should be experimentally obtained with FD-NIRS or TD-NIRS¹⁰, due to device limitations, it was not possible in this project. Hence, in our research, the DPF was determined by the wavelengths of the fNIRS device and age of the participant. (Duncan et al., 1996). According to Duncan et al. (1996), the DPF for two wavelengths can be calculated with the formulae:

$$DPF_{744} = 5.11 + 0.106 \cdot Age^{0.723} \quad (2.5.1)$$

$$DPF_{852} = 4.67 + 0.062 \cdot Age^{0.819} \quad (2.5.2)$$

with age given in years.

Duncan et al. (1996) developed a broadband radiofrequency-modulated phase-resolved spectroscopy (PRS) instrument using four wavelengths(690, 744, 807, and 832 nm) which can measure phase shifts through more than 4 cm of brain tissue in less than one second. In the study, the modulation frequency was set at 200 MHz, which has been shown theoretically to be a frequency at which phase shift and true mean optical path length are equal (Arridge et al., 1992). By dividing the true mean optical path length with source-detector separation, the DPF can be obtained.

The authors also provided mathematical models based on the measurements. The estimated DPF is in sequential order as the used wavelengths. The shorter the wavelength, the larger the mean DPF they measured. Even though only four equations were provided with the above-mentioned four wavelengths, and our wavelengths were different than that of the authors used, we were convinced that with the above two equations, we could still get a fair estimate of the true DPF in our case.

¹⁰FD-NIRS and TD-NIRS stand for frequency domain NIRS and time domain NIRS respectively. In principle, both fast modulation techniques, FD and TD, allow the obtaining of absolute chromophore concentration quantities. However, this comes at the price of the greatly increased complexity of the instrumentation and the analysis. As a consequence, most commercial systems use the CW-NIRS technique.

Source: <https://nirx.net/cwfnirs>
visited in September 2022.

Methods

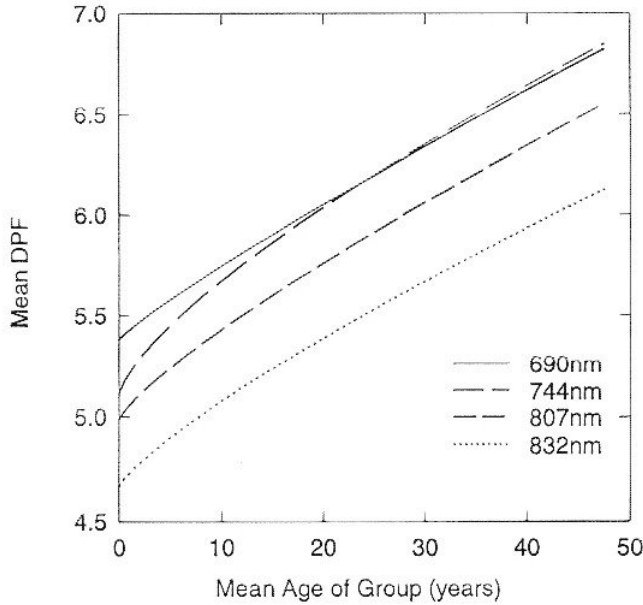


Figure 2.9: Age dependence of DPF. Taken from Duncan et al. (1996)

It is important to note that the noise due to motion artifacts, drift, broadband noise, heartbeat, and respiration artifacts need to be processed before the concentration was estimated, according to the previous research (Huppert et al., 2009).

Later on, the extracerebral component in long channels should be reduced by using measurements from the short channels as follows: the first principal components from the two short channels were estimated and then multiplied by its coefficient from the general linear model (GLM) (Friston et al., 1994). However, this was not done in the present study, since the coefficient from the GLM were very small. They were of the magnitudes 10^{-16} , whereas the hemodynamic response in the long channels was of the magnitudes 10^{-5} . Hence, we concluded the extracerebral components in our case could be negligible.

Channels with unusable data were excluded here for further analysis. The scalp coupling index (SCI) (Pollonini et al., 2013) is a common measure to detect unusable channels. The SCI estimates the correlation between the two wavelength channels in the cardiac band as follows.

First, the signal is bandpass-filtered to keep only the cardiac band. In our case, a wide band of (0.5 - 2.5) Hz was chosen. Then, amplitude normalization is performed, and the SCI computation is defined as the absolute cross-correlation value at zero-time lag (Pollonini et al., 2013).

2.5 Data Processing

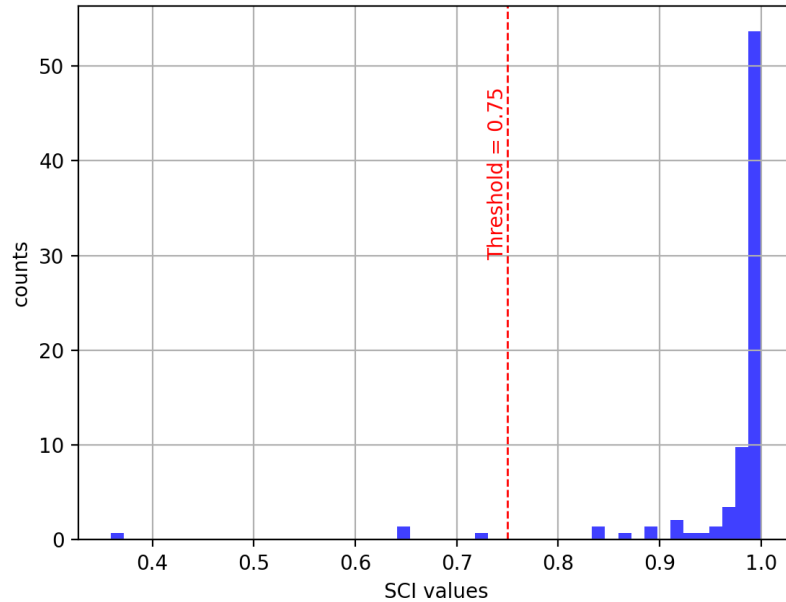


Figure 2.10: Distribution of SCI values.

In the present study, only four channels failed to reach the threshold of 0.75. In other words, of all the measurements (14 channels per participant, 8 participants in total). Over 96% of the measurements passed the SCI threshold.

Chapter 3

Results

From our measurements, the results varied a lot individually. Hence, the grand average and further statistical analysis would not be well-applicable. In this section, individual results from selected participants are presented, including waveform morphology of the 14-channel measurements for both the HbO and HbR data. In addition, the regional analysis for the HbO data is also included in this section. Results from other measured participants are put in Appendix D.

First of all, our channels with the optode template are defined as shown in figure 3.1.

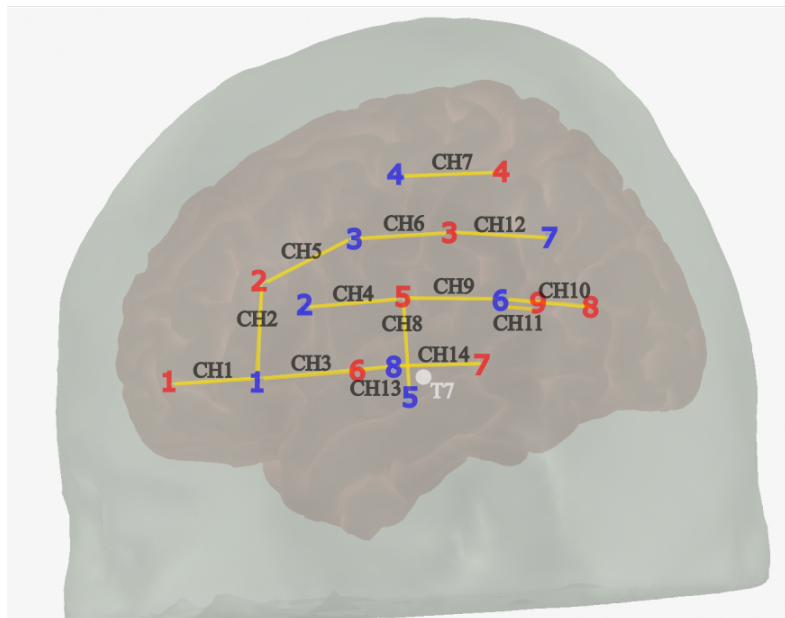


Figure 3.1: Channel Definition

Our regions of interest (ROI) were defined as the following figure. The auditory cortex was in particular of our interest. Hence, channel 4, channel 8, and channel 9 together formed one region (ROI 2). The rest of the channels formed ROI 1. It was of our interest to compare how the responses of the auditory cortex differ from the rest of the left brain hemisphere.

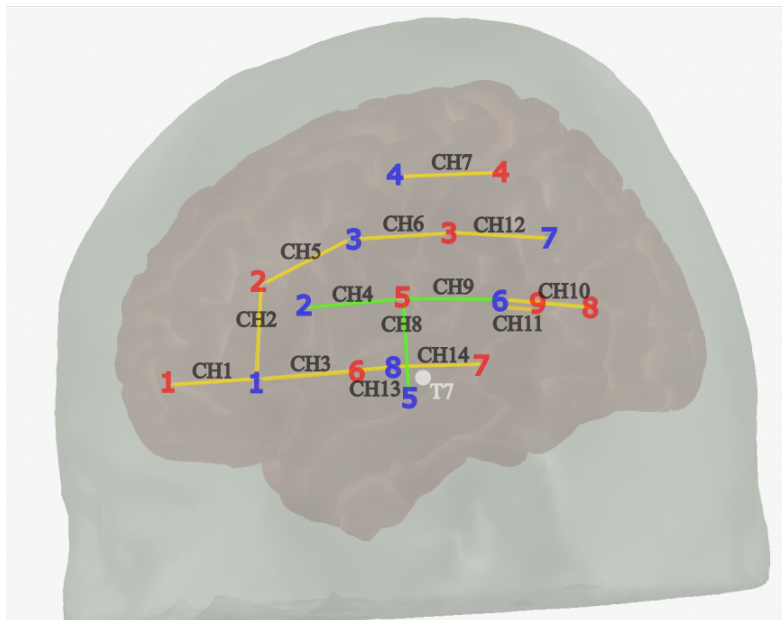


Figure 3.2: ROI Definition

In the following plots, channels with invalid SCI are not taken into consideration, and hence are not shown. Measurements in all channels are plotted on the same scale except for the two short channels, i.e. Channel 11 and 13, marked in thicker outlines. In all our measurements, the change in the dynamic hemoglobin responses was significantly less in the short channels by more than a magnitude.

Results

3.1 Participant 3

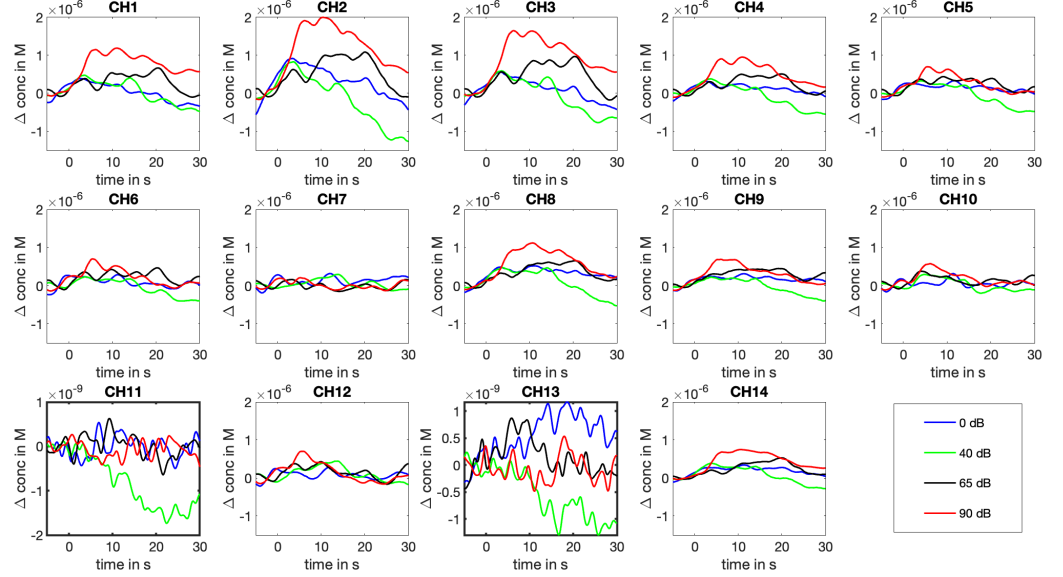


Figure 3.3: HbO Measurement from participant 3.

Lines represent the block-averaged results over eight epochs. The averaged change in HbO concentration (in Mole) is plotted from 5 seconds before the start of the auditory stimuli to 30 seconds after the start of the stimuli. Four colors are used to differentiate the responses from sound stimuli of different intensity levels.

For the HbO waveform morphology (Figure 3.3), tonic responses could be observed in channels 1, 2, and 3, and phasic responses could be observed in channels 10 and 12.¹ The sound stimuli of the greatest intensity resulted in the largest response in terms of magnitude in all the long channels.

The HbR measurement (Figure 3.4) also showed separation from responses to stimuli of different SPLs. In most of the channel measurements, the loudest sound stimuli caused the most negative change in HbR concentration after 20 seconds from the start of sound stimuli.

The averaged responses from each channel (Figure 3.5) are very similar in the two defined regions in terms of both waveform and magnitude.

¹Tonic response refers to a sustained response, which activates during the course of the stimulus; while phasic response refers to a transient response with one or few action potentials at the onset of stimulus followed by accommodation. (Wang et al., 2014)

3.1 Participant 3

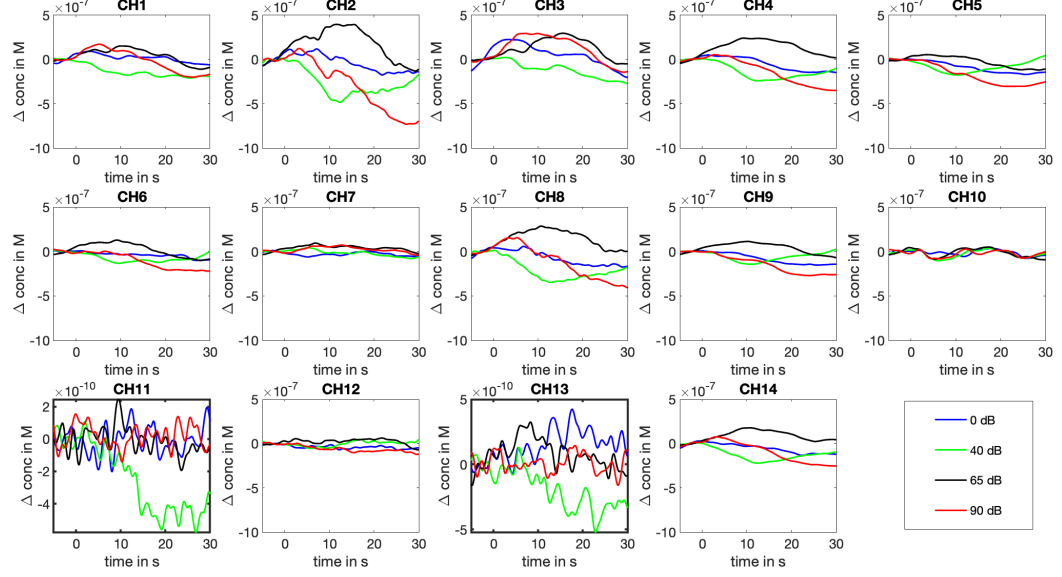


Figure 3.4: HbR Measurement from participant 3.

Lines represent the block-averaged results over eight epochs. The averaged change in HbR concentration (in Mole) is plotted from 5 seconds before the start of the auditory stimuli to 30 seconds after the start of the stimuli. Four colors are used to differentiate the responses from sound stimuli of different intensity levels.

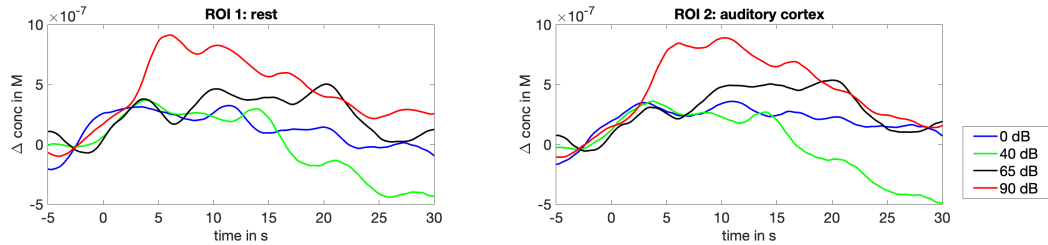


Figure 3.5: ROI Measurement from participant 3.

In every channel, the block-averaged HbO response over eight epochs was taken first before the mean HbO response in the whole region was calculated. The averaged change in HbO concentration (in Mole) for channels in the region is plotted from 5 seconds before the start of the auditory stimuli to 30 seconds after the start of the stimuli. Four colors are used to differentiate the response from sound stimuli of different intensity levels.

Out of the results from all participants, the results from this participant were the closest the results reported by Weder et al (2018).

Results

3.2 Participant 4

There were also some poor measurements even though the SCI is above the threshold of 0.75. For example, in our case of participant 4, almost all channels showed barely any response except for channel 14, in which the measured data also appeared to be noisy. One potential reason was due to the thick dark hair of the participant that resulted in more light absorption, which affected the result greatly.

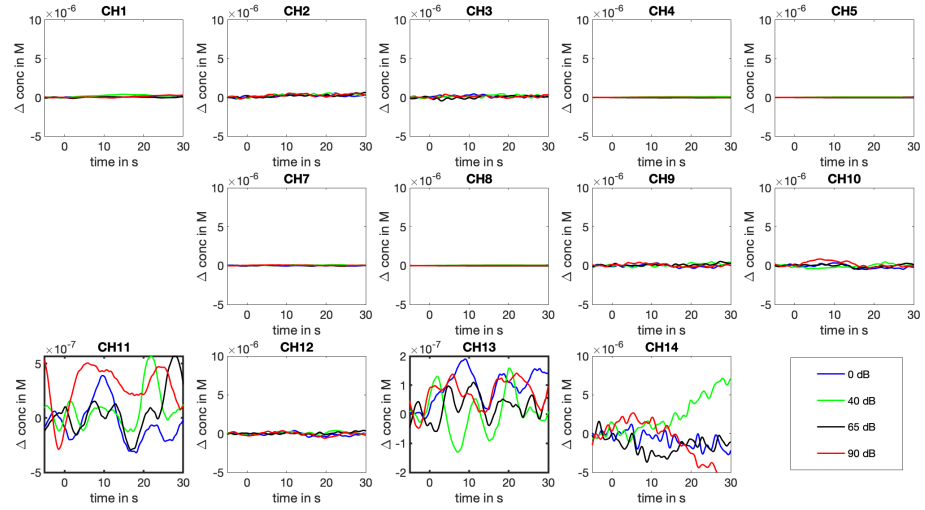


Figure 3.6: HbO Measurement from participant 4.

Lines represent the block-averaged results over eight epochs. The averaged change in HbO concentration (in Mole) is plotted from 5 seconds before the start of the auditory stimuli to 30 seconds after the start of the stimuli. Four colors are used to differentiate the responses from sound stimuli of different intensity levels.

3.2 Participant 4

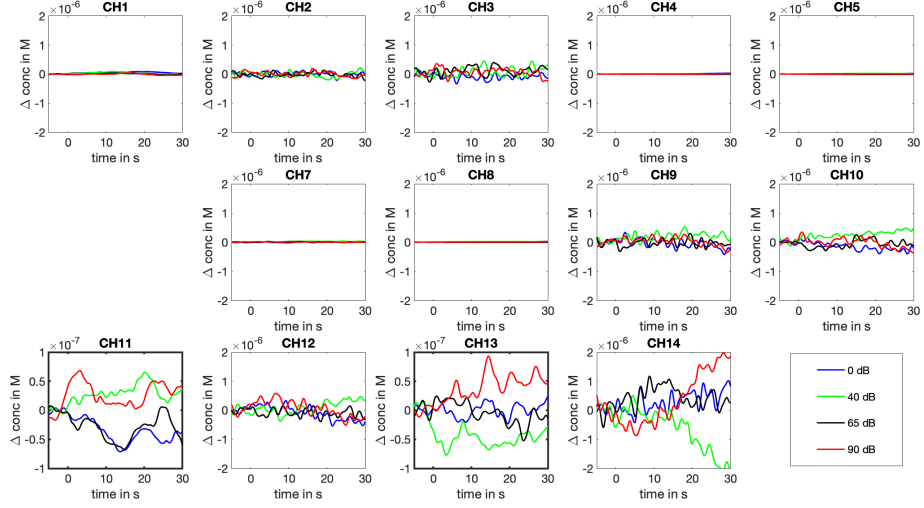


Figure 3.7: HbR Measurement from participant 4.

Lines represent the block-averaged results over eight epochs. The averaged change in HbR concentration (in Mole) is plotted from 5 seconds before the start of the auditory stimuli to 30 seconds after the start of the stimuli. Four colors are used to differentiate the responses from sound stimuli of different intensity levels.

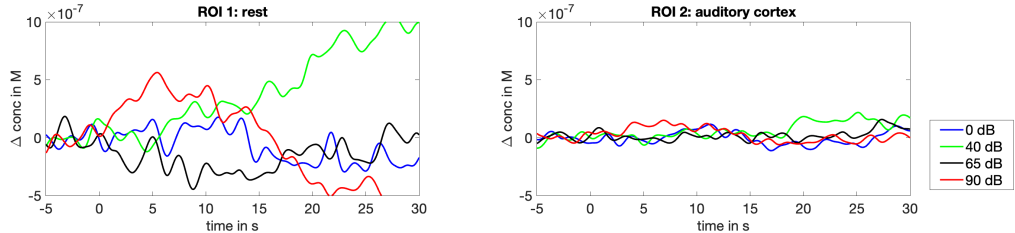


Figure 3.8: ROI Measurement from participant 4.

In every channel, the block-averaged HbO response over eight epochs was taken first before the mean HbO response in the whole region was calculated. The averaged change in HbO concentration (in Mole) for channels in the region is plotted from 5 seconds before the start of the auditory stimuli to 30 seconds after the start of the stimuli. Four colors are used to differentiate responses from sound stimuli of different intensity levels.

Results

3.3 Participant 5

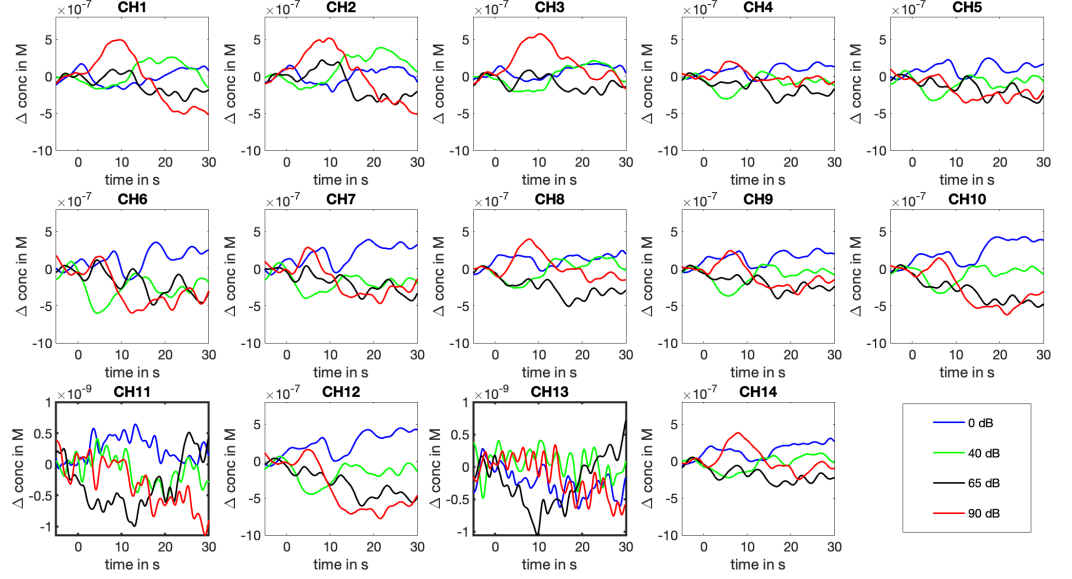


Figure 3.9: HbO Measurement from participant 5.

Lines represent the block-averaged results over eight epochs. The averaged change in HbO concentration (in Mole) is plotted from 5 seconds before the start of the auditory stimuli to 30 seconds after the start of the stimuli. Four colors are used to differentiate the responses from sound stimuli of different intensity levels.

For the HbO waveforms (Figure 3.9), there were significantly larger on-sets for the 90 dB sound stimuli in channels 1, 2, and 3, i.e. around the Broca's area.

Apart from this, the HbR waveforms (Figure 3.10) were also quite different from the ones Weder et al (2018). reported. For the loudest sound stimuli, channels overlying the caudal superior temporal gyrus and channels over Broca's area showed clear phasic responses.

The averaged responses from each channel (Figure 3.11) were very similar in the two defined regions in terms of both waveform and magnitude.

3.3 Participant 5

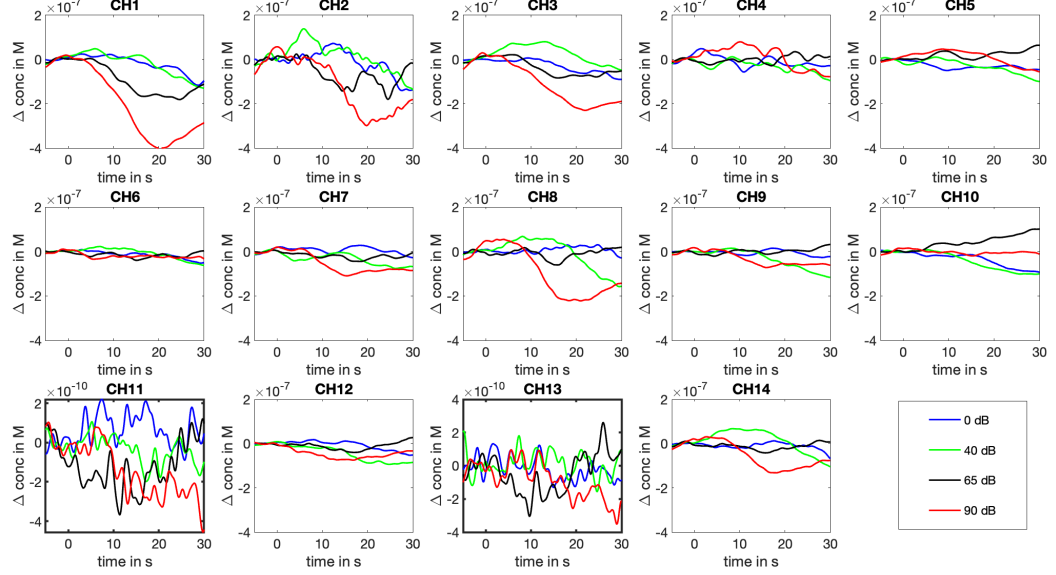


Figure 3.10: HbR Measurement from participant 5.

Lines represent the block-averaged results over eight epochs. The averaged change in HbR concentration (in Mole) is plotted from 5 seconds before the start of the auditory stimuli to 30 seconds after the start of the stimuli. Four colors are used to differentiate the responses from sound stimuli of different intensity levels.

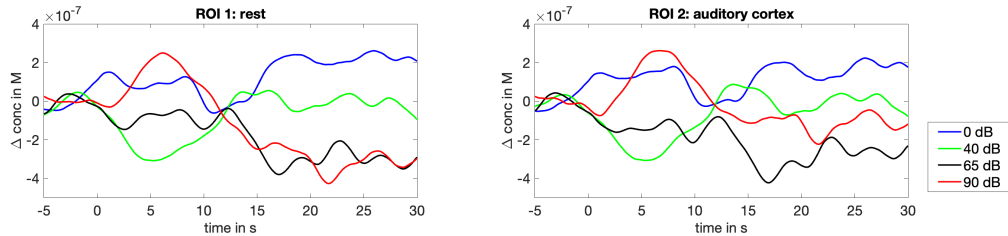


Figure 3.11: ROI Measurement from participant 5.

In every channel, the block-averaged HbO response over eight epochs was taken first before the mean HbO response in the whole region was calculated. The averaged change in HbO concentration (in Mole) for channels in the region is plotted from 5 seconds before the start of the auditory stimuli to 30 seconds after the start of the stimuli. Four colors are used to differentiate the responses from sound stimuli of different intensity levels.

Results

3.4 Participant 7

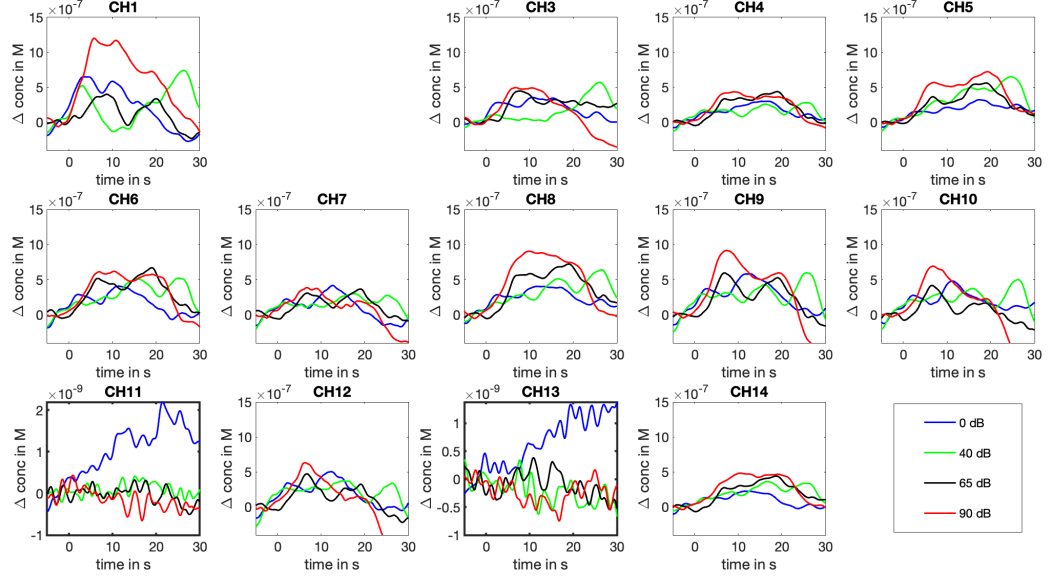


Figure 3.12: HbO Measurement from participant 7.

Lines represent the block-averaged results over eight epochs. The averaged change in HbO concentration (in Mole) is plotted from 5 seconds before the start of the auditory stimuli to 30 seconds after the start of the stimuli. Four colors are used to differentiate the responses from sound stimuli of different intensity levels.

The results from this participant were indeterminant to differentiate between responses to different sound pressure levels. From the HbO measurement (Figure 3.12), only measurement from channel 1 showed a significant difference between results from the loudest sound stimuli and other quieter sound stimuli.

It is noteworthy to notice that the change in HbR concentration (Figure 3.12) from this participant was also positive in most of the channels. However, the magnitude was significantly smaller than that of the HbO concentration change of the same participant.

The averaged responses from each channel (Figure 3.14) were very similar in the two defined regions in terms of the waveform. Larger magnitude were recorded in ROI 2.

3.4 Participant 7

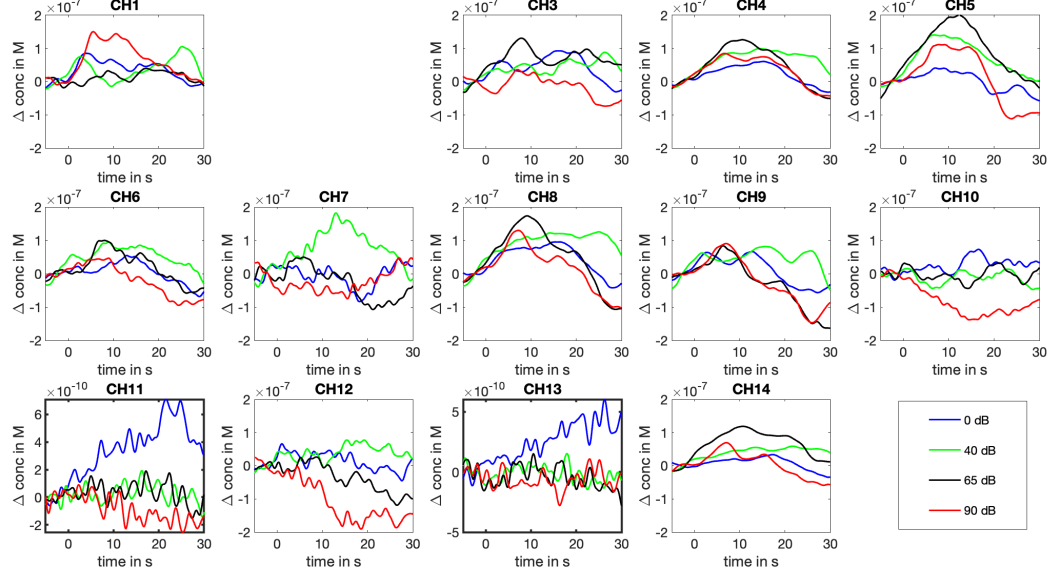


Figure 3.13: HbR Measurement from participant 7.

Lines represent the block-averaged results over eight epochs. The averaged change in HbR concentration (in Mole) is plotted from 5 seconds before the start of the auditory stimuli to 30 seconds after the start of the stimuli. Four colors are used to differentiate the responses from sound stimuli of different intensity levels.

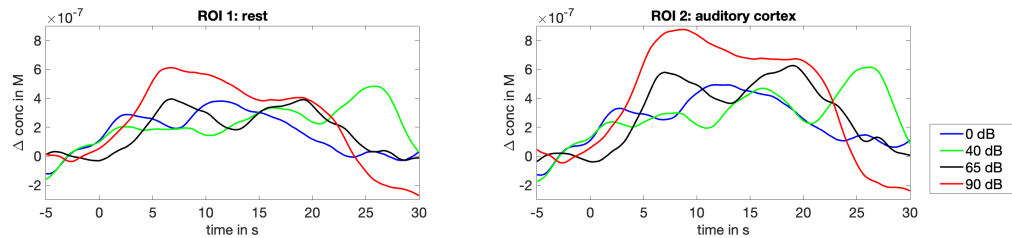


Figure 3.14: ROI Measurement from participant 7.

In every channel, the block-averaged HbO response over eight epochs was taken first before the mean HbO response in the whole region was calculated. The averaged change in HbO concentration (in Mole) for channels in the region is plotted from 5 seconds before the start of the auditory stimuli to 30 seconds after the start of the stimuli. Four colors are used to differentiate the responses from sound stimuli of different intensity levels.

Chapter 4

Discussion

4.1 Waveform Morphology

The results we got for the waveform morphology did not speak entirely with the results that Weder et al. (2018) reported. In most of the cases, larger sound pressure levels did result in greater positive changes in oxygenated hemoglobin concentration, or in other words, greater negative changes in de-oxygenated hemoglobin concentration. However, the results were not consistent between participants. The separation between different sound pressure levels could not be clearly seen. Apart from the results with the loudest auditory stimuli, responses from other quieter auditory stimuli were rather indistinguishable. Moreover, regarding the type of responses we measured from different regions of the left brain hemisphere, phasic responses could be observed from the channels over the supramarginal superior temporal gyrus from most of the participants. However, only from some of the participants, channels over Broca's area could show a broad tonic pattern as Weder et al. (2018) described.

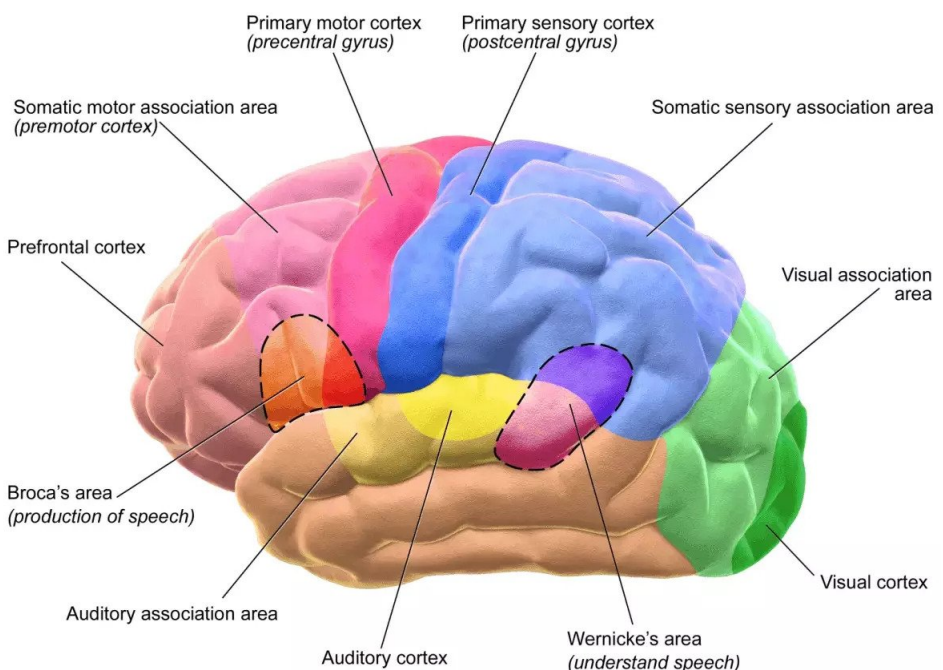
4.2 Regional Analysis

In comparison to the research from Weder et al. (2018), we chose a different approach to define our region of interest. Instead of first looking at the results and grouping different regions according to similar waveforms, we were more interested to know how the responses from the auditory cortex would be compared with other regions of the measured left brain hemisphere, so we grouped the three channels over the caudal superior temporal gyrus as one region (ROI 2), and the rest of the channels as another region (ROI 1).

The auditory cortex 4.1 was our interest in this study. It is around the

4.3 Device Limitation and fNIRS Testing Conditions

caudal superior temporal gyrus. We compared the hemoglobin response from the three channels over the auditory cortex with all the other channels lying on the rest of the measured left brain hemisphere. The waveform morphology of the auditory cortex is very similar to the counterparts of the rest of the measured parts. In other words, the dynamic hemoglobin response of the auditory cortex represents that of the entire left brain hemisphere fairly well.



Source: <https://human-memory.net/sensory-cortex/>

Figure 4.1: Motor and sensory regions of the cerebral cortex

4.3 Device Limitation and fNIRS Testing Conditions

There were several factors that potentially caused the results from this project to vary from that Weder et al. (2018) reported. First, we used the device Brite23. It is also a continuous-wave fNIRS device. The sources emitted light of slightly different wavelengths, which are 757 nm and 843 nm, whereas Weder et al. (2018) used the device (NIRScout, NIRX, Germany) which sources emitted light of wavelengths 760 nm and 850 nm. Additionally, as for the fNIRS testing procedure, we could have also improved on several

Discussion

things. To begin with, a darker sound-attenuating booth would be more suitable. In our setup, the testing was also performed in a sound-attenuating cabin, but with normal light conditions. Still, if the lighting was dimmer, there could be less noise in the hemoglobin response from visual stimulation. In addition, it would make sense to stabilize the participant’s neck with a neck cushion. Not only would it be more comfortable for the participants during the measurement. Motion artifacts could also be reduced. Moreover, by including breaks in between, participants might be able to maintain better attention.

Also, from our measurements, data from female participants with long hair had worse data quality. In our configuration, since we were only measuring the left brain hemisphere. First asking the participant to put the hair to the right side made it easier to put the cap on. Sometimes when the participants had thick long hair, trying to put the hair aside can be a futile attempt, but it was easier when they first put the hair to the other side. Last but not least, we would be curious to know how the hemoglobin responses from more people are like. If possible, more participants should be measured so the results from the project can be more credible. For example, participants of different ages and every gender and race would be desirable for this hearing research. Besides, other than only measuring normal-hearing people, it would also be of great interest to measure some cochlear implant users and compare the results together.

4.4 Data Processing

Our measured data was processed with a modified approach. In the research from Weder et al. (2018), data pre-processing and analysis was executed in MATLAB and SPSS (version 24, IBM Corp., USA). They combined custom-made MATLAB scripts with Homer2 (Huppert et al., 2009) functions. On the other hand, the newer Homer3 (Huppert et al., 2009) with our MATLAB script in this study. Judging from the varying individual results, group analysis or statistical analysis will not be applicable in this case. Hence, the software program for statistical analysis, SPSS, was not used in this project. Furthermore, the differential path length factor (DPF) for each participant was calculated from their age. The resultant HbO and HbR concentration was estimated with the correction factor, whereas Weder et al. (2018) did not mention how they chose or calculated the DPF values.

4.5 Loudness Perception

In this project, results from individuals varied much. Although in hearing research, the response from normal-hearing participants are often similar and reproducible, it is also well-known that, even among normal-hearing listeners, considerable differences still exist in loudness perceptions (Garnier et al., 1999). More recent research (Weder et al., 2020) was conducted in detail, and showed that brain activation in response to different stimulus intensities is more reliant upon individual loudness sensation than the physical stimulus properties. Therefore, the authors suggested that loudness estimates should be examined when interpreting results, especially when it comes to measurements using different auditory stimulus intensities. Different loudness perception can explain the varying results from individual participants.

4.6 Intelligibility of the Auditory Stimuli

ICRA noises were chosen as the stimuli in this study because it is believed to be able to activate broad cortical auditory areas. However, some other studies were able to detect differences in cortical responses to the speech of different intelligibility. Pollonini et al. (2013) found that normal speech evoked stronger responses within the auditory cortex than distorted speech did, and environmental sounds produced the least cortical activation. ICRA noises are amplitude-modulated noises, are completely unintelligible, and thus, belong to the distorted-speech category. Although ICRA noises may be able to activate broader cortical auditory areas compared to a simple static stimulus, normal speech can perhaps produce even stronger responses within the auditory cortex, according to Pollonini et al. (2013). In addition, by providing intelligible normal speech as a stimulus rather than unintelligible noise, the measurement process can be less boring for the participants. They can then be more compliant and thus maintain better attention to actively listen to the soundtracks.

4.7 Language Processing in Human Brains

One primary goal of fNIRS research is to improve a patient's ability to discriminate speech. In many studies, topics associated with hearing and language processing were investigated. However, language perception and processing in the human brain do not have to be involved with auditory stimuli. Visual-only speech can also activate language processing in the human brain. Shader et al. (2021) used both auditory-only and visual-only

Discussion

connected speech as stimuli in their research. Their results suggested that Heschl's gyrus (see Figure 4.2) may be the most advantageous location for identifying hemodynamic responses to complex auditory speech signals using fNIRS, for measuring responses to visual speech with fNIRS, regions corresponding to the facial processing pathway in the occipital lobe can be more advantageous.

4.8 Laterality of Brain Activation

In the present study, the fNIRS optodes were all placed on the left brain hemisphere, since according to Frost et al. (1999), language processing is strongly left lateralized. Nonetheless, from other papers, different results were observed and did not speak entirely with the conclusion from Frost et al. (1999). For example, the data from Pollonini et al. (2013) is more responsive to changes in activation within the right hemisphere. Belin et al. (2000) showed that the voice-selective regions can be found bilaterally along the upper bank of STS. Shader et al. (Shader et al., 2021) also measured relatively symmetrical patterns across both hemispheres. Hence, if it is more advantageous to measure the left hemisphere for cortical response to audiometric stimuli with fNIRS remains till this point a question to be answered.

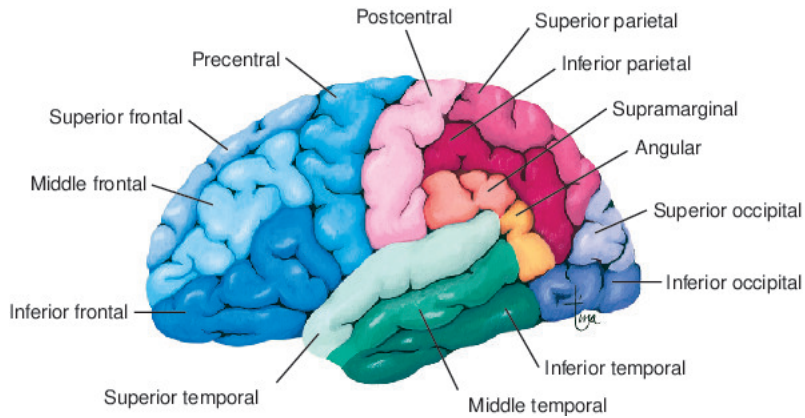
4.9 Depth and Location of Cortical Response

The depth of cortical response to complex auditory speech signals can also greatly affect the fNIRS measurements. Strangman et al. (2013) demonstrated that sensitivity in depth decreases exponentially and diminishing returns appear to begin around 40 to 50 mm source-detector separations.

The left inferior frontal gyrus (see Figure 4.2), or more specifically Broca's area (see Figure 4.1) is implicated in higher-level linguistic processing (Belin et al., 2000). While in some studies (Wijayasiri et al., 2017) (Zhou et al., 2018), significant cortical activity in response to auditory speech signals in this region can be detected, it was not always the case (Mushtaq et al., 2019). The studies that observed significant activation in the frontal region used fMRI or a combination of fMRI and fNIRS. It is possible that speech-evoked activity in the inferior frontal gyrus is isolated to the deeper cortical areas, so it's less likely to be detected with fNIRS. Different neuroimaging methods can also explain why some studies (Frost et al., 1999) reported language processing to be left-lateralized whereas in other studies (Shader

4.10 HbR and HbO Data

et al., 2021), opposite results were observed. It is possible that speech-evoked activities are related to the deeper cortical areas in the left hemisphere while the stimuli evoked responses in more superficial areas of the right cortex, making them more easily detected by fNIRS.



Source: <https://www.tabers.com/tabersonline/view/Tabers-Dictionary/734639/all/gyrus>

Figure 4.2: Gyrus

4.10 HbR and HbO Data

Most fNIRS studies only present HbO data (Ferrari and Quaresima, 2012), since it has a lower noise level, and thus more obvious responses can be observed. However, with our system, no significant difference was found regarding the HbO and HbR noise levels for most of the participants. Only some channels were measured with higher noise levels for the HbR data collected from participant 6. Unlike what Weder et al. (2018) presented in their paper, we were surprised to be able to measure comparably the same magnitude of HbO and HbR responses.

Chapter 5

Conclusion and Future Prospectives

This study aims to confirm and reproduce the results from Weder et al. (2018). With the limited devices, we made our measurement conditions, i.e. optode template configuration and audio sound stimuli as similar as those of the previous research from Weder et al. (2018) as possible.

Our results were not completely as expected. Few common patterns could be found between participants. Therefore, we analysed the results from each individual participant and compared these with the results Weder et al. (2018) provided. Variables that might have potentially affected the results of the study were investigated with a thorough literature review.

Other than purely attempting to reproduce the results from the one main paper (Weder et al., 2018), this study also takes other related research into consideration. We studied and considered the effect of different auditory stimuli, individual perception of the loudness of the sound, depth, laterality, and location of the cortical activation. By taking advantage of previous fMRI studies (Belin et al., 2000) (Belin et al., 2002) (Hall et al., 2001) (Frost et al., 1999), we compared the laterality of cortical activation in this study and previous research. Building upon the presumption from earlier research and our measurement data, we also concluded that the cortical activation from auditory stimuli is possibly deeper for some participants in the auditory cortex. Additionally other than merely taking the HbO data for analysis, the magnitude and noise of the measured HbR data were also compared with the counterparts of the HbO data.

In this study, only normal-hearing adults were enrolled in order to best deline the capabilities of fNIRS in this straightforward situation. Nevertheless, a long-term goal of this research is to use fNIRS to objectively evaluate how auditory stimuli relay to the auditory cortex in deaf subjects before and after

cochlear implantation. The vision is to be able to use fNIRS in clinical applications to identify and intervene in hearing loss earlier in child development. Hence, we hope to include more subjects which not only include normal-hearing adults but also cochlear implant users and children. A comparison between normal-hearing adults and other groups can provide value in this field of study. Additionally, it would also be of our interest to investigate the cortical response with fNIRS when subjects are given other different stimuli, e.g. visual-only stimuli, normal-speech stimuli, or musical stimuli.

Appendix A

Acronym

Acronyms

BOLD blood-oxygen-level-dependent.

CW-NIRS continuous wave near-infrared spectroscopy.

DPF differential path length factor.

FD-NIRS frequency domain near-infrared spectroscopy.

fMRI functional magnetic resonance imaging.

fNIRS functional near-infrared spectroscopy.

GLM general linear model.

HbO oxygenated hemoglobin.

HbR deoxygenated hemoglobin.

ICRA International Collegium for Rehabilitative Audiology.

LSL lab streaming layer.

mBLL modified Beer-Lambert law.

PCA principle component analysis.

PRS phase-resolved spectroscopy.

ROI region of interest.

SCI scalp coupling index.

SPL sound pressure level.

Acronyms

STS superior temporal sulcus.

TD-NIRS time domain near-infrared spectroscopy.

Appendix B

List of Figures

List of Figures

1.1	Anatomical terminology.	5
2.1	Probe design from Weder et al. (2018)	7
2.2	Probe design in this research. The original view is shown here in AtlasViewer. The red numbers represent the light sources and the blue numbers represent the detector. Channels are shown in yellow lines. For better readability, our channel definition will be shown later in the report in another edited picture (Figure 3.1) from AtlasViewer.	7
2.3	The 10-10 international system of EEG electrode placement. T7 is the left 10% position between A1 and A2 through the central Cz.	8
2.4	SDgui interface and optode coordinates.	9
2.5	Manufacturing process of the cap	10
2.6	Finished cap on dummy	10
2.7	fnIRS Device: Brite23	13
2.8	Flow chart of data processing steps	14
2.9	Age dependence of DPF. Taken rom Duncan et al. (1996) . .	16
2.10	Distribution of SCI values.	17
3.1	Channel Definition	18
3.2	ROI Definition	19
3.3	HbO Measurement from participant 3.	20
3.4	HbR Measurement from participant 3.	21
3.5	ROI Measurement from participant 3.	21
3.6	HbO Measurement from participant 4.	22
3.7	HbR Measurement from participant 4.	23
3.8	ROI Measurement from participant 4.	23
3.9	HbO Measurement from participant 5.	24
3.10	HbR Measurement from participant 5.	25
3.11	ROI Measurement from participant 5.	25

List of Figures

3.12 HbO Measurement from participant 7	26
3.13 HbR Measurement from participant 7	27
3.14 ROI Measurement from participant 7	27
4.1 Motor and sensory regions of the cerebral cortex	29
4.2 Gyrus	33
D.1 HbO measurement from participant 1	44
D.2 HbR measurement from participant 1	45
D.3 ROI measurement from participant 1	45
D.4 HbO measurement from participant 2	46
D.5 HbR measurement from participant 2	47
D.6 ROI measurement from participant 2	47
D.7 HbO Measurement from participant 6	48
D.8 HbR Measurement from participant 6	49
D.9 ROI Measurement from participant 6	49
D.10 HbO measurement from participant 8. Silent comparison . . .	50
D.11 HbR measurement from participant 8. Silent comparison . . .	51
D.12 ROI measurement from participant 8. Silent comparision. . .	51

Appendix C

List of Tables

List of Tables

2.1 Demographic information of the study participants.	6
--	---

Appendix D

Other Measurement Data

D.1 Participant 1

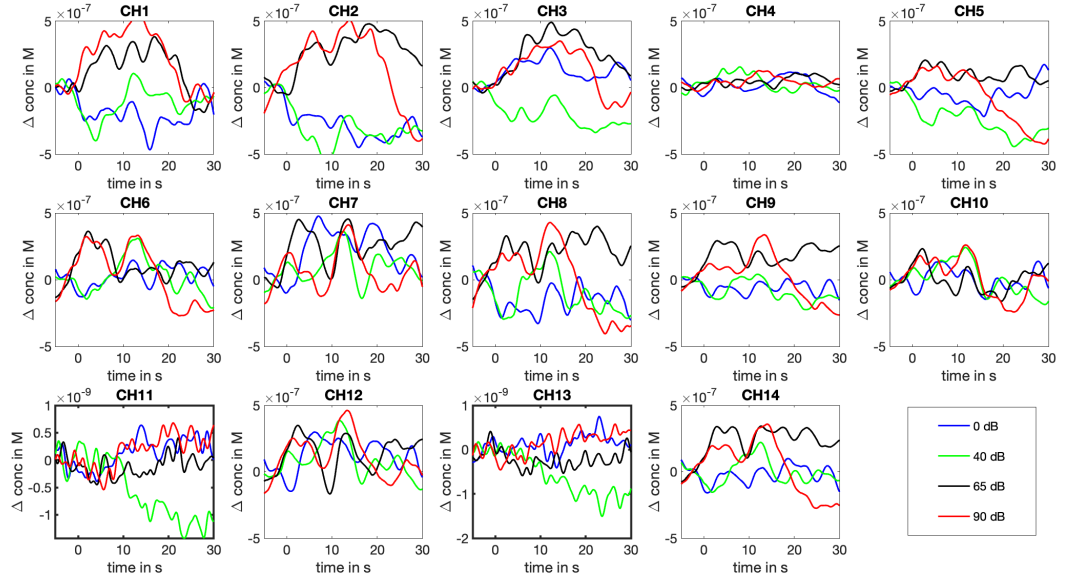


Figure D.1: HbO measurement from participant 1.

Lines represent the block-averaged results over eight epochs. The averaged change of HbO concentration (in Mole) is plotted from 5 seconds before the start of the auditory stimuli to 30 seconds after the start of the stimuli. Four colours are used to differentiate the response from sound stimuli of different intensity levels.

D.1 Participant 1

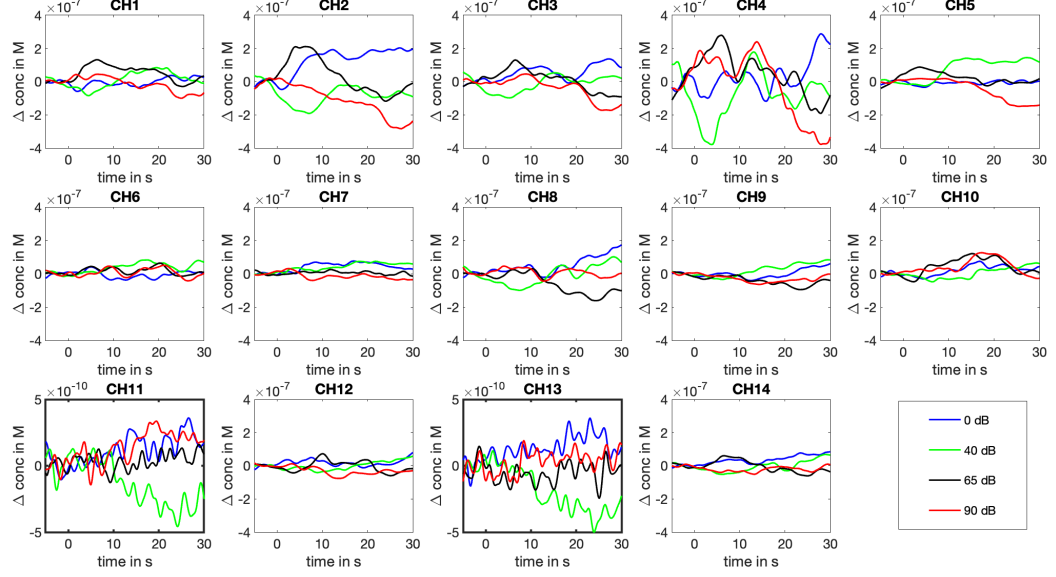


Figure D.2: HbR measurement from participant 1.

Lines represent the block-averaged results over eight epochs. The averaged change of HbR concentration (in Mole) is plotted from 5 seconds before the start of the auditory stimuli to 30 seconds after the start of the stimuli. Four colours are used to differentiate the response from sound stimuli of different intensity levels.

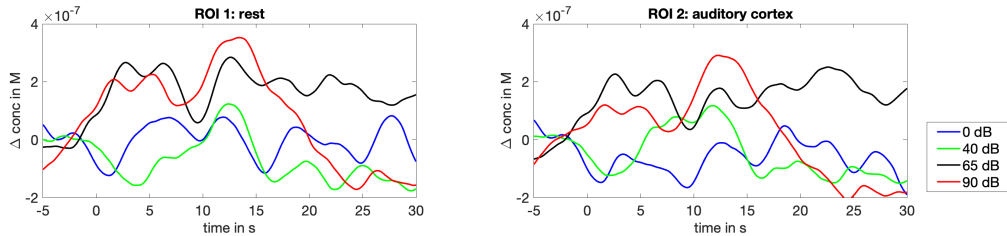


Figure D.3: ROI measurement from participant 1.

Other Measurement Data

D.2 Participant 2

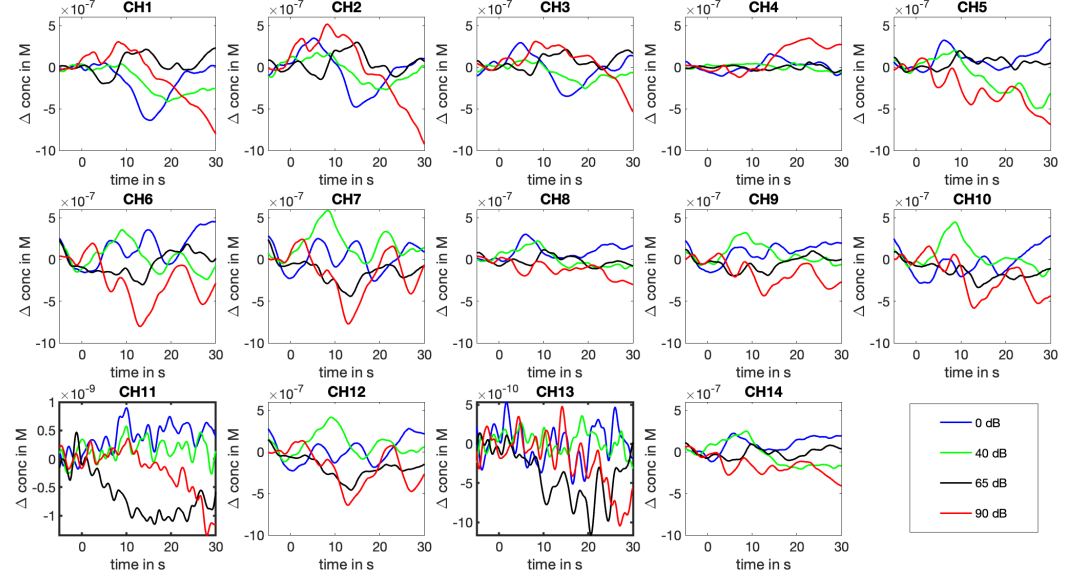


Figure D.4: HbO measurement from participant 2.

Lines represent the block-averaged results over eight epochs. The averaged change of HbO concentration (in Mole) is plotted from 5 seconds before the start of the auditory stimuli to 30 seconds after the start of the stimuli. Four colours are used to differentiate the response from sound stimuli of different intensity levels.

D.2 Participant 2

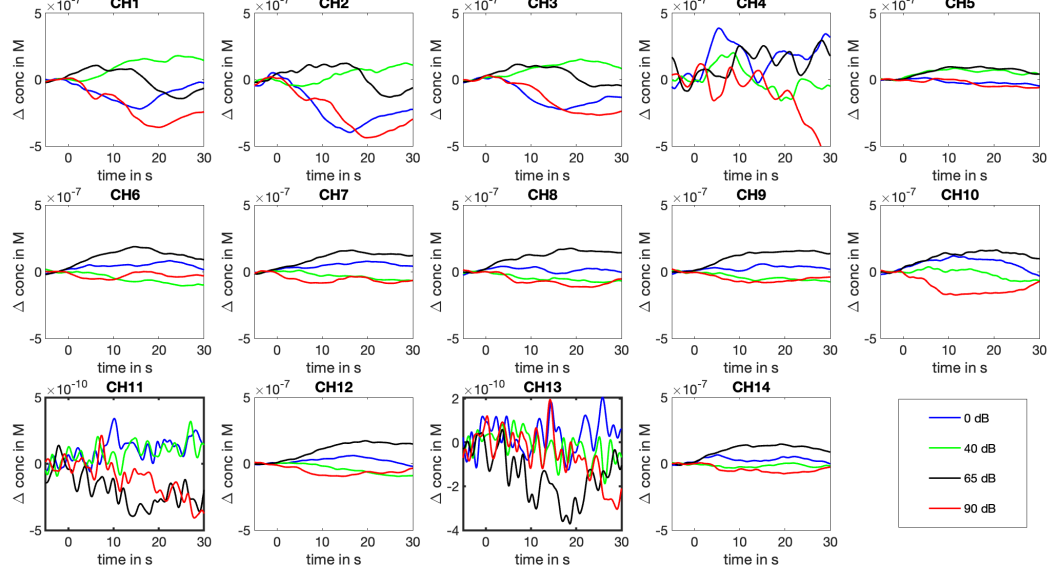


Figure D.5: HbR measurement from participant 2.

Lines represent the block-averaged results over eight epochs. The averaged change of HbR concentration (in Mole) is plotted from 5 seconds before the start of the auditory stimuli to 30 seconds after the start of the stimuli. Four colours are used to differentiate the response from sound stimuli of different intensity levels.

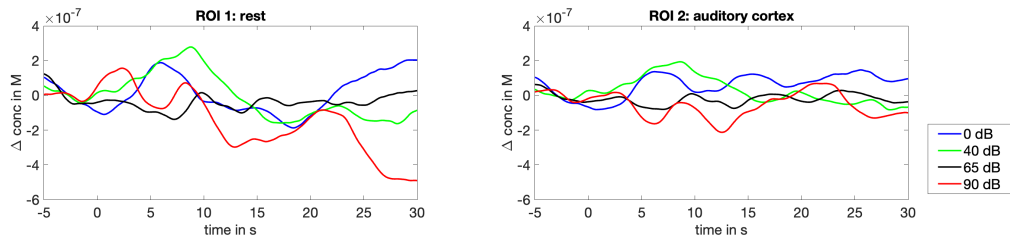


Figure D.6: ROI measurement from participant 2.

Other Measurement Data

D.3 Participant 6

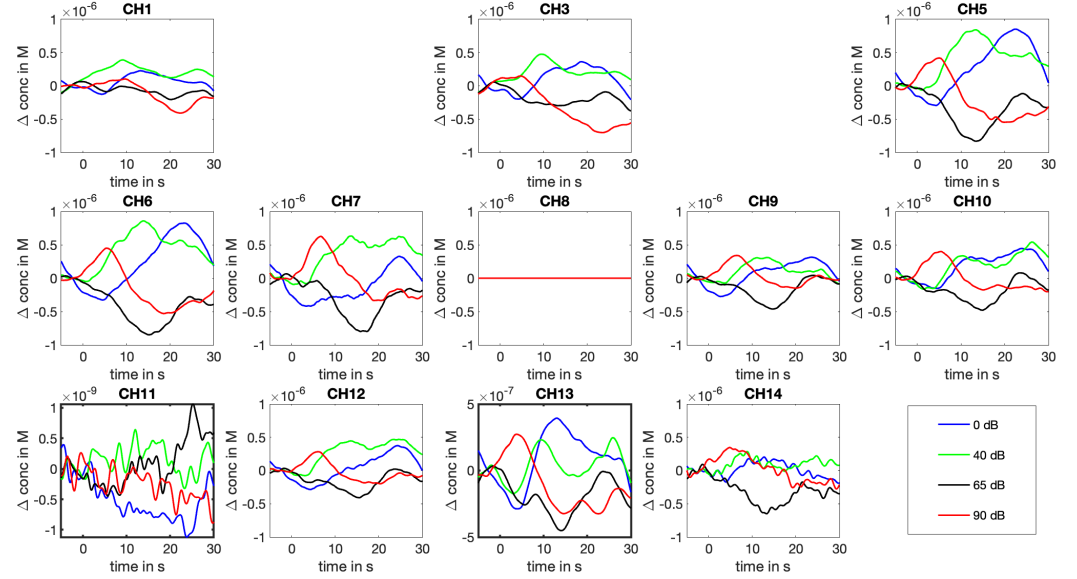


Figure D.7: HbO Measurement from participant 6.

Lines represent the block-averaged results over eight epochs. The averaged change of HbO concentration (in Mole) is plotted from 5 seconds before the start of the auditory stimuli to 30 seconds after the start of the stimuli. Four colours are used to differentiate the response from sound stimuli of different intensity levels.

D.3 Participant 6

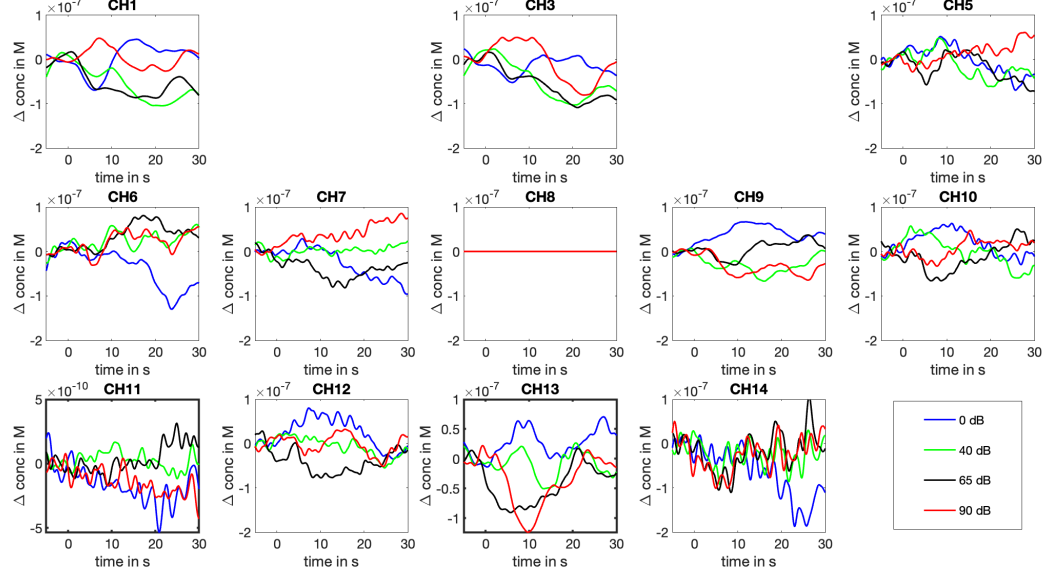


Figure D.8: HbR Measurement from participant 6.

Lines represent the block-averaged results over eight epochs. The averaged change of HbR concentration (in Mole) is plotted from 5 seconds before the start of the auditory stimuli to 30 seconds after the start of the stimuli. Four colours are used to differentiate the response from sound stimuli of different intensity levels.

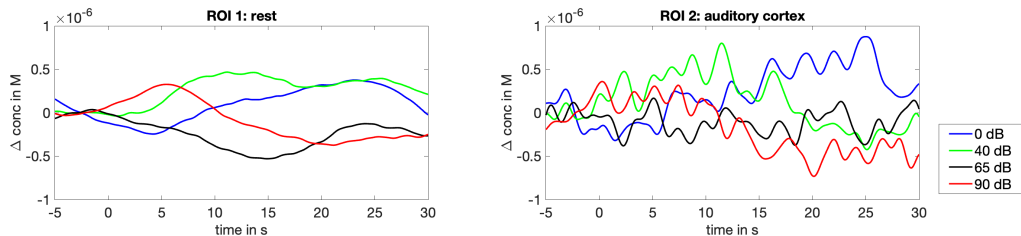


Figure D.9: ROI Measurement from participant 6.

For the oxygenated hemoglobin, HbO waveform, the loudest sound stimuli resulted in phasic response for almost all the channels. In addition, it also resulted in faster on-set compared with other stimuli of lower sound pressure levels.

On the other hand, as for the deoxygenated hemoglobin, HbR response, results from multiple channels appeared to be noisy even if the SCI values were already above the suggested threshold.

Other Measurement Data

D.4 Participant 8

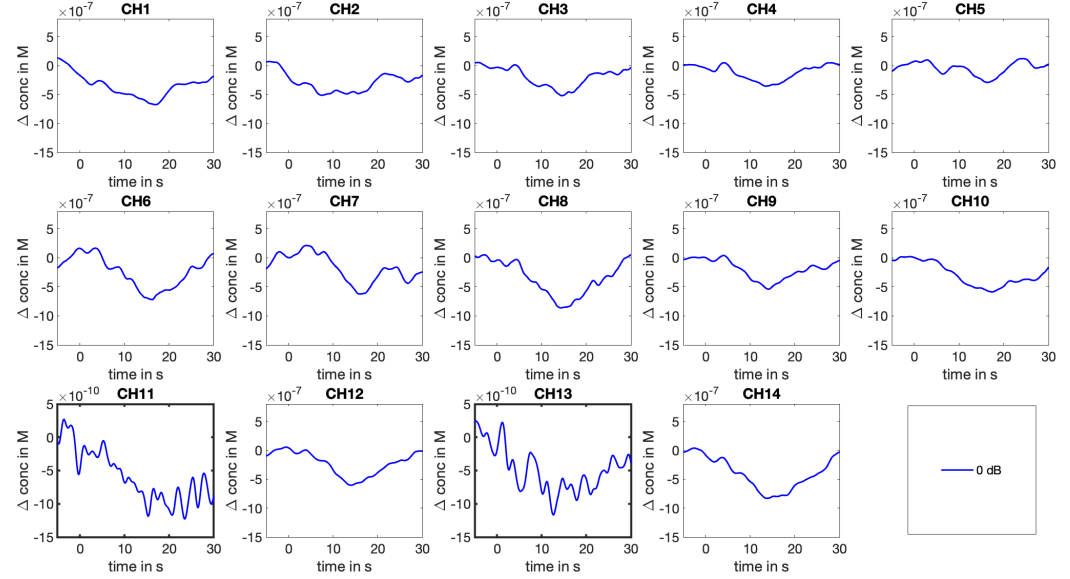


Figure D.10: HbO measurement from participant 8. Silent comparison

Lines represent the block-averaged results over eight epochs. The averaged change of HbO concentration (in Mole) is plotted from 5 seconds before the start of the auditory stimuli to 30 seconds after the start of the stimuli.

D.4 Participant 8

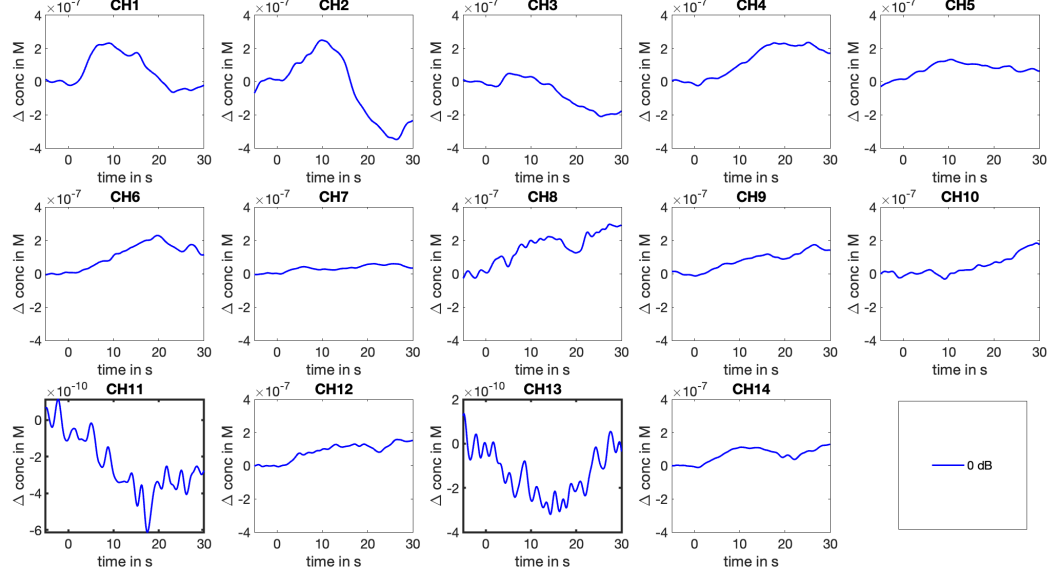


Figure D.11: HbR measurement from participant 8. Silent comparison

Lines represent the block-averaged results over eight epochs. The averaged change of HbR concentration (in Mole) is plotted from 5 seconds before the start of the auditory stimuli to 30 seconds after the start of the stimuli.

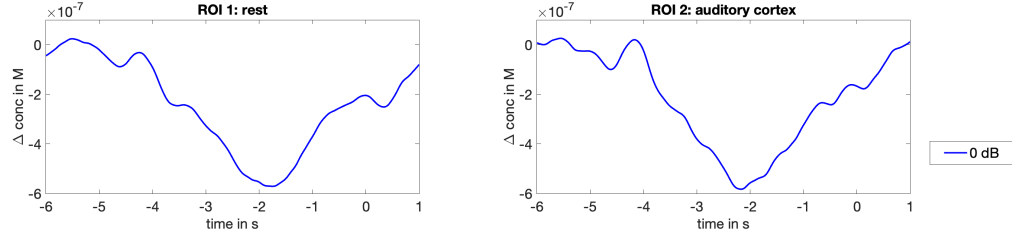


Figure D.12: ROI measurement from participant 8. Silent comparision.

This participant was given only silence stimuli. No pattern could be concluded for the measured waveform morphology. Nonetheless, it is noteworthy to know that even if there were almost no visual and sound stimuli, dynamic hemoglobin response still presented.

Bibliography

- Aasted, C. M., Yücel, M. A., Cooper, R. J., Dubb, J., Tsuzuki, D., Becerra, L., Petkov, M. P., Borsook, D., Dan, I., and Boas, D. A. (2015). Anatomical guidance for functional near-infrared spectroscopy: AtlasViewer tutorial. *Neurophotonics*, 2(2):020801.
- Arridge, S. R., Cope, M., and Delpy, D. T. (1992). The theoretical basis for the determination of optical pathlengths in tissue: temporal and frequency analysis. *Physics in Medicine and Biology*, 37(7):1531–1560.
- Belin, P., Zatorre, R., and Ahad, P. (2002). Human temporal-lobe response to vocal sounds. *Brain research. Cognitive brain research*, 13:17–26.
- Belin, P., Zatorre, R., Lafaille, P., Ahad, P., and Pike, B. (2000). Voice-selective areas in human auditory cortex. *Nature*, 403:309–12.
- Chan, D., Fourcin, A., Gibbon, D., Granstrom, B., Hucvale, M., George, K., Kvale, K., Lamel, L., Lindberg, B., Moreno, A., Mouropoulos, J., and Senia, F. (1995). Eurom - a spoken language resource for the eu. *Proc. Eurospeech*, 1.
- Clark, B. A. (2000). First-and second-language acquisition in early childhood.
- Delpy, D. T., Cope, M., van der Zee, P., Arridge, S., Wray, S., and Wyatt, J. (1988). Estimation of optical pathlength through tissue from direct time of flight measurement. *Physics in Medicine and Biology*, 33(12):1433–1442.
- Dreschler, W., Herschuure, H., Ludvigsen, C., and Westermann, S. (2001). Icra noises: Artificial noise signals with speech-like spectral and temporal properties for hearing aid assessment. *Audiology*, 40:148–157.
- Duncan, A., Meek, J., Clemence, M., Elwell, C. E., Fallon, P., Tyszczuk, L., Cope, M., and Delpy, D. T. (1996). Measurement of cranial optical path length as a function of age using phase resolved near infrared spectroscopy. *Pediatric Research*, 39:889–894.

Bibliography

- Ferrari, M. and Quaresima, V. (2012). A brief review on the history of human functional near-infrared spectroscopy (fnirs) development and fields of application. *NeuroImage*, 63(2):921–935.
- Friston, K. J., Holmes, A. P., Worsley, K. J., Poline, J.-P., Frith, C. D., and Frackowiak, R. S. (1994). Statistical parametric maps in functional imaging: a general linear approach. *Human brain mapping*, 2(4):189–210.
- Frost, J. A., Binder, J. R., Springer, J. A., Hammeke, T. A., Bellgowan, P. S., Rao, S. M., and Cox, R. W. (1999). Language processing is strongly left lateralized in both sexes. evidence from functional MRI. *Brain*, 122 (Pt 2):199–208.
- Garnier, S., Micheyl, C., Berger-Vachon, C., and Collet, L. (1999). Effect of signal duration on categorical loudness scaling in normal and in hearing-impaired listeners. *Audiology : official organ of the International Society of Audiology*, 38:196–201.
- Hall, D., Haggard, M., Summerfield, A., Akeroyd, M., Palmer, A., and Bowtell, R. (2001). Functional magnetic resonance imaging measurements of sound-level encoding in the absence of background scanner noise. *The Journal of the Acoustical Society of America*, 109:1559–70.
- Huppert, T. J., Diamond, S. G., Franceschini, M. A., and Boas, D. A. (2009). Homer: a review of time-series analysis methods for near-infrared spectroscopy of the brain. *Appl. Opt.*, 48(10):D280–D298.
- Jöbsis, F. F. (1977). Noninvasive, infrared monitoring of cerebral and myocardial oxygen sufficiency and circulatory parameters. *Science*, 198(4323):1264–1267.
- Molavi, B. and Dumont, G. A. (2012). Wavelet-based motion artifact removal for functional near-infrared spectroscopy. *Physiological Measurement*, 33(2):259–270.
- Mushtaq, F., Wiggins, I., Kitterick, P., Anderson, C., and Hartley, D. (2019). Evaluating time-reversed speech and signal-correlated noise as auditory baselines for isolating speech-specific processing using fnirs. *PLOS ONE*, 14:e0219927.
- Newport, E. L. (1990). Maturational constraints on language learning. *Cognitive Science*, 14(1):11–28.

Bibliography

- Pelphrey, K. A. (2013). *Blood-Oxygen-Level-Dependent (BOLD) Signal*, pages 465–466. Springer New York, New York, NY.
- Pollonini, L., Olds, C., Abaya, H., Bortfeld, H., Beauchamp, M., and Oghalai, J. (2013). Auditory cortex activation to natural speech and simulated cochlear implant speech measured with functional near-infrared spectroscopy. *Hearing research*, 309.
- Robinshaw, H. M. (1995). Early intervention for hearing impairment: Differences in the timing of communicative and linguistic development. *British Journal of Audiology*, 29(6):315–334. PMID: 8861408.
- Shader, M., Luke, R., Gouailhardou, N., and McKay, C. (2021). The use of broad vs restricted regions of interest in functional near-infrared spectroscopy for measuring cortical activation to auditory-only and visual-only speech. *Hearing Research*, 406:108256.
- Strangman, G. E., Li, Z., and Zhang, Q. (2013). Depth sensitivity and source-detector separations for near infrared spectroscopy based on the colin27 brain template. *PLOS ONE*, 8(8):1–13.
- Swinehart, D. F. (1962). The beer-lambert law. *Journal of Chemical Education*, 39(7):333.
- Wang, L., Liang, P.-J., Zhang, P.-M., and Qiu, Y.-H. (2014). Ionic mechanisms underlying tonic and phasic firing behaviors in retinal ganglion cells. *Channels*, 8:298 – 307.
- Weder, S., Shoushtarian, M., Olivares, V., Zhou, X., Innes-Brown, H., and McKay, C. (2020). Cortical fnirs responses can be better explained by loudness percept than sound intensity. *Ear and Hearing*, 41:1.
- Weder, S., Zhou, X., Shoushtarian, M., Innes-Brown, H., and McKay, C. (2018). Cortical processing related to intensity of a modulated noise stimulus-a functional near-infrared study. *J. Assoc. Res. Otolaryngol.*, 19(3):273–286.
- Wijayasiri, P., Hartley, D., and Wiggins, I. (2017). Brain activity underlying the recovery of meaning from degraded speech: A functional near-infrared spectroscopy (fnirs) study. *Hearing Research*, 351.
- Yoshinaga-Itano, C., Sedey, A., Coulter, D., and Mehl, A. (1998). Language of early- and later-identified children with hearing loss. *Pediatrics*, 102:1161–71.

Bibliography

Zhou, X., Seghouane, A.-K., Shah, A., Innes-Brown, H., Cross, W., Litovsky, R., and McKay, C. M. (2018). Cortical speech processing in postlingually deaf adult cochlear implant users, as revealed by functional near-infrared spectroscopy. *Trends in Hearing*, 22:2331216518786850. PMID: 30022732.

Bibliography

Erklärung der Selbstständigkeit

Hiermit versichere ich, die vorliegende Arbeit selbstständig verfasst und keine anderen als die angegebenen Quellen und Hilfsmittel benutzt sowie die Zitate deutlich kenntlich gemacht zu haben.

.....
Ort, Datum

Pei-Yi Lin